ISSN 1949-8470 (online)

World Journal of *Radiology*

World J Radiol 2022 April 28; 14(4): 70-106

Published by Baishideng Publishing Group Inc

World Journal of Radiology

Contents

Monthly Volume 14 Number 4 April 28, 2022

MINIREVIEWS

ORIGINAL ARTICLE

Retrospective Cohort Study

Retrospective Study

LETTER TO THE EDITOR

World Journal of Radiology

Monthly Volume 14 Number 4 April 28, 2022

Contents

NAME OF JOURNAL
World Journal of Radiology

ISSN
ISSN 1949-8470 (online)

LAUNCH DATE
January 31, 2009

FREQUENCY
Monthly

EDITORS-IN-CHIEF
Thomas J Vogl

EDITORIAL BOARD MEMBERS
https://www.wjgnet.com/1949-8470/editorialboard.htm

PUBLICATION DATE
April 28, 2022

INSTRUCTIONS TO AUTHORS
https://www.wjgnet.com/bpg/gerinfo/204

GUIDELINES FOR ETHICS DOCUMENTS
https://www.wjgnet.com/bpg/GerInfo/287

GUIDELINES FOR NON-NATIVE SPEAKERS OF ENGLISH
https://www.wjgnet.com/bpg/gerinfo/240

PUBLICATION ETHICS
https://www.wjgnet.com/bpg/GerInfo/288

PUBLICATION MISCONDUCT
https://www.wjgnet.com/bpg/gerinfo/208

ARTICLE PROCESSING CHARGE
https://www.wjgnet.com/bpg/gerinfo/242

STEPS FOR SUBMITTING MANUSCRIPTS
https://www.wjgnet.com/bpg/GerInfo/239

ONLINE SUBMISSION
https://www.f6publishing.com

World Journal of Radiology

Submit a Manuscript: https://www.f6publishing.com

World J Radiol 2022 April 28; 14(4): 70-81

DOI: 10.4329/wjr.v14.i4.70

ISSN 1949-8470 (online)

MINIREVIEWS

Focal liver lesions in cirrhosis: Role of contrast-enhanced ultrasonography

Tommaso Vincenzo Bartolotta, Angelo Randazzo, Eleonora Bruno, Adele Taibbi

Specialty type: Radiology, nuclear medicine and medical imaging

Provenance and peer review: Invited article; Externally peer reviewed.

Peer-review model: Single blind

Peer-review report's scientific quality classification

Grade A (Excellent): 0
Grade B (Very good): 0
Grade C (Good): 0
Grade D (Fair): D
Grade E (Poor): 0

P-Reviewer: Ren J, China

Received: February 25, 2021
Peer-review started: February 25, 2021
First decision: May 3, 2021
Revised: May 16, 2021
Accepted: April 8, 2022
Article in press: April 8, 2022
Published online: April 28, 2022

Tommaso Vincenzo Bartolotta, Angelo Randazzo, Eleonora Bruno, Adele Taibbi, Department of Radiology, University Hospital "Paolo Giaccone", Palermo 90127, Italy

Tommaso Vincenzo Bartolotta, Department of Radiology, Fondazione Istituto G. Giglio Hospital, Cefalù 90015, Italy

Corresponding author: Tommaso Vincenzo Bartolotta, MD, PhD, Associate Professor, Department of Radiology, University Hospital "Paolo Giaccone", Section of Radiology, Department BiND, Palermo 90127, Italy. tommasovincenzo.bartolotta@unipa.it

Abstract

Contrast-enhanced ultrasound (CEUS) represents a great innovation for the evaluation of focal liver lesions (FLLs). The main advantage of CEUS is the real-time imaging examination and the very low toxicity in patients with renal failure. Liver cirrhosis has been recognized as a major risk factor for the onset of hepatocellular carcinoma (HCC) and intrahepatic cholangiocarcinoma (ICC). HCC in liver cirrhosis develops as the last step of a complex that leads to the gradual transformation from regenerative nodule through dysplastic nodule to HCC. In patients with liver cirrhosis, a surveillance program is recommended consisting of ultrasound (US) for detecting small focal lesions. A wide spectrum of benign and malignant lesions other than HCC may be found in the cirrhotic liver and their differentiation is important to avoid errors in staging diseases that may preclude potentially curative therapies. Several published studies have explored the value of CEUS in liver cirrhosis and they have been shown to have excellent diagnostic and prognostic performances for the evaluation of non-invasive and efficient diagnosis of FLLs in patients at high risk for liver malignancies. The purpose of this article is to describe and discuss CEUS imaging findings of FLLs including HCC and ICC, all of which occur in cirrhotic livers with varying prevalence.

Key Words: Ultrasonography; Contrast-enhanced ultrasound; Liver cirrhosis; Liver neoplasms; Hepatocellular carcinoma; Focal liver lesions

Core Tip: Contrast-enhanced ultrasound (CEUS) represents a breakthrough in the evaluation of focal liver lesions (FLLs). Currently, CEUS is included as a part of the suggested diagnostic work-up of FLLs in cirrhotic patients and in their follow-up for an accurate assessment of therapeutic response. After a brief description of the basis of different CEUS techniques, several liver lesions that can be found in the cirrhotic liver including benign, malignant or pseudo-lesions, will be described and discussed on the basis of our experience and literature data.

Citation: Bartolotta TV, Randazzo A, Bruno E, Taibbi A. Focal liver lesions in cirrhosis: Role of contrast-enhanced ultrasonography. *World J Radiol* 2022; 14(4): 70-81
URL: https://www.wjgnet.com/1949-8470/full/v14/i4/70.htm
DOI: https://dx.doi.org/10.4329/wjr.v14.i4.70

INTRODUCTION

Liver cirrhosis

Liver cirrhosis represents the final stage of chronic inflammation through the establishment of necrosis and fibrogenesis up to a total subversion of the hepatic parenchyma and it has systemic repercussions and a fatal outcome in the absence of a liver transplant. Liver cirrhosis is the 14th most common cause of death worldwide[1].

Etiologically, liver cirrhosis recognizes infectious causes (hepatitis B, hepatitis C, schistosoma japonicum), autoimmune (primary biliary cirrhosis, autoimmune hepatitis, primary sclerosing cholangitis), alcohol abuse, metabolic causes (Wilson disease, hemochromatosis) and vascular or cryptogenic causes[2]. The combination of imaging and serological investigation (transaminases and cholestasis indices) is often sufficient for the diagnosis; however, the gold standard remains the liver biopsy which also allows physicians to identify the noxa that led to the stage of cirrhosis[1]. In the clinical setting, ultrasound (US) allows a morphological assessment of the liver and portal circulation. US also plays a major role as the recommended tool for surveillance every 6 mo at early detection of small hepatocellular carcinoma (HCC)[3].

Imaging characterization of focal lesions in cirrhosis is crucial for appropriate patient management[4, 5]. To this end, US is a non-specific technique used to characterize focal liver lesions (FLLs).

Contrast-enhanced ultrasound

At the end of the 1990s, the introduction of contrast agents based on intravenous microbubbles to contrast-specific gray-scale US techniques has enabled contrast-enhanced ultrasonography (CEUS) to represent macro-vascularity and also microcirculation (vessels up to 40 μm). Starting in the 2000s, the advent of low-solubility gas bubbles (like sulfur hexafluoride) with phospholipid shells for their flexibility has led to a full real time CEUS examination[6].

CEUS, throughout the vascular phase with its blood-pool contrast agent, allows real-time recording with non-invasive assessment of liver perfusion without resorting to expensive and not very common equipment such as Computed Tomography (CT) or Magnetic Resonance Imaging (MRI) that require the use of ionizing radiation or nephrotoxic contrast agents. OF note, when gas microbubbles are injected into the vein, they remain in the intravascular space (blood-pool agents), Only one of marketed contras agents shows a late phase with uptake by hepatic Kupffer cells (Table 1)[7].

CEUS is safe and well tolerated: Renal or pulmonary diseases do not present contraindications for this use and no blood tests are needed to check kidney function. In a study of about 23000 patients, less than 0.01% of the patient population reported a serious adverse event with no death events[8].

Actually, CEUS is included in the diagnostic work-up of FLLs detected in the healthy population and to study metastases in patients with cancer and to identify HCC in cirrhotic patients, allowing for better management of the disease with effective and advantageous therapies[9-10]. A recent meta-analysis showed that specificity and sensitivity for CEUS in the characterization of FLLs were respectively 87% and 92%[10]. CEUS is gaining an increasing role in the imaging work-up of HCC and many international guidelines are now considering CEUS as a diagnostic tool for HCC as well as CT and MRI with encouraging results and is positive in terms of the cost-benefit analysis[11-12]. Based on literature data and our experience in our center, the recent innovations in the CEUS of FLLs in cirrhotic patients will be presented and discussed.

TECHNICAL NOTE

The US cases illustrated in this article are acquired through various ultrasound equipment provided

Table 1 Characteristics of contrast agents SonoVue and Sonazoid for contrast-enhanced ultrasound

Agent	SonoVue	Sonazoid
Gas	Sulfurhexafluoride (SF_6)	Perfluorobutane (C_4F_{10})
Envelope	Monolayer of phospholipid (DSPC, DPPG-Na)	Monolayer of phospholipid (Hydrogenated egg phosphatidyl serine Na)
MI	Low MI (< 0.1)	Intermediate MI (> 0.2)
Mean size	1.5-2.5 μm	2.3-2.9 μm
Distribution after injection	Pure blood pool agent	Blood pool agent with uptake by hepatic Kupffer cells after 1 min by injection

DSPC: 1,2-distearoyl-sn-glycero-3-phosphocholine; DPPG-Na: 1,2-dipalmitoyl-sn-glycero-3-phospho-rac-glycerol sodium; MI: Mechanical index.

with multifrequency convex array probes and contrast-specific imaging software: MyLab Twice (Esaote, Genova, Italy), RS80A and RS85A (Samsung Medison, Co. Ltd., Seoul, Korea) and iU22 unit (Philips Ultrasound, Bothell, WA, USA). Before the injection of bolus contrast, a standard exam together with color/power and pulsed Doppler valuation was always performed to optimize lesion images and define the best plane for its visualization. The contrast agent used was composed of gas microbubbles filled with sulfur hexafluoride (SonoVue, Bracco, Milan, Italy) that was injected using a 20- or 22-gauge needle in a cubital vein and a 2.4-mL bolus with a 5-10 ml of saline flush. Low mechanical index (MI) from 0.05 to 0.08 and low frame rate (5 Hz) were used for real-time imaging to avoid microbubble breakdown. The level of the lesion was the focus of examination and the duration of each exam was about 5 min after contrast agent injection.

The digital cine-loops were acquired before and after performing the contrast at different times in the arterial phase (from 10 s to 35 s after the injection), portal phase (from 55 s to 80 s after the injection) and delayed phase (from 235 s to 260 s after the injection).

Basal echogenicity and the dynamic modality of enhancement of each lesion in all vascular phases and among the near liver parenchyma were compared.

CIRRHOTIC NODULES

Liver cirrhosis has been recognized as a major risk factor for the onset of HCC and intrahepatic cholangiocarcinoma (ICC) compared to the non-cirrhotic population, of 30 and 20 times, respectively[13]. In the management of hepatic nodules in liver cirrhosis, early diagnosis and treatment is mandatory. HCC in liver cirrhosis develops as the last step of a complex, multi-step hepatocarcinogenesis process during several molecular and tissue alterations leading to the gradual transformation from regenerative nodule (RN) through low- and high-grade dysplastic nodule (DN) to HCC[14]. Changes of intranodular blood supply is the main transformation for imaging diagnosis: RN show similar blood supply to a normal liver. As a consequence, RNs are typically non-hypervascular. They can be seen as numerous tiny hypoechoic or hyperechoic nodules throughout the liver on grayscale US whereas at CEUS they usually are iso-enhancing to the adjacent liver parenchyma throughout the vascular phase, even if they may show transient hypo-vascularity in the arterial phase[4] (Figure 1).

DN are the next step towards HCC. Often multiple, DNs are classified as low or high grade according to the presence of cytological atypia. These borderline lesions show wide variations of blood supply with overlaps of vascular supply between DN and well-differentiated HCC, with the vast majority of RN and DN being isoechoic to the adjacent liver parenchyma in portal venous and late phase at CEUS [15].

Of note, in a study encompassing 215 FLLs in cirrhotic patients and comparing the CEUS features of RN and DN, 95.1% of RN lesions showed delayed or simultaneous enhancement in the arterial phase in comparison to surrounding liver parenchyma. On the other hand, DN lesions resembled this contrast-enhancement pattern only partially, due to the presence of intralesional areas of arterial enhancement followed by a wash out in the late phase. In pathology, these areas of arterial contrast-enhancement within the DN have proven to be early HCC[16]. Hence, any enhancement in the arterial phase within a nodule should be regarded as suspicious for HCC, resembling a "nodule in a nodule" appearance.

MALIGNANT LESIONS

Hepatocellular carcinoma

HCC is the fifth most common cancer in men and the ninth in women showing a greater incidence in developing countries where over 80% of all estimated new cases worldwide occurred in 2012[17].

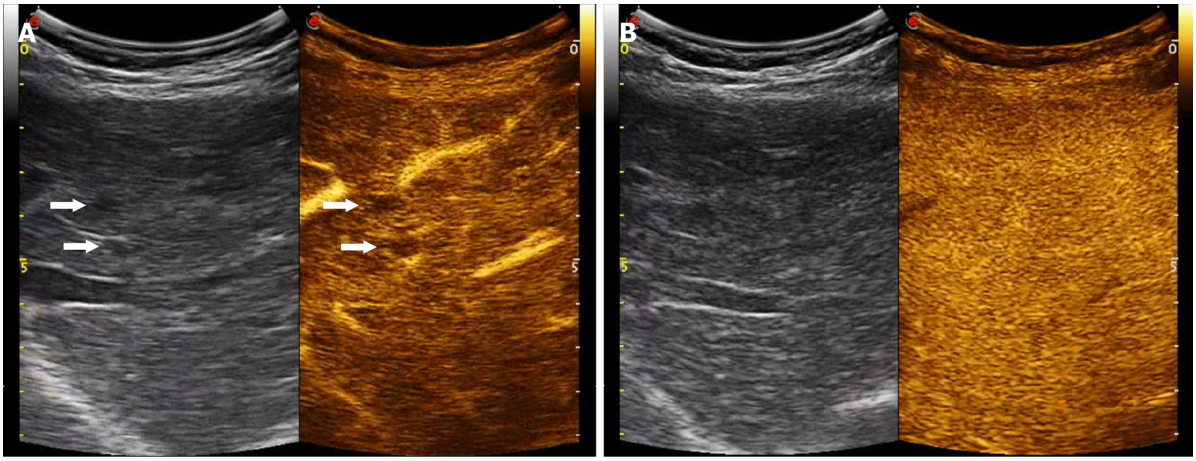

DOI: 10.4329/wjr.v14.i4.70

Figure 1 Regenerative nodule. A: Contrast-enhanced ultrasound examination in the arterial phase (29 s after the i.v. injection of contrast agent) shows two millimetric hypoechoic nodules, showing lack of contrast enhancement (right, arrows); B: In the late phase (142 s after the injection) both nodules are isoechoic to the adjacent liver parenchyma.

Almost 90% of HCCs originate through a stepway progression from RN to HCC which may take place in a quite variable period, even though it may take only a few months[18]. On the other hand, the estimated doubling time of HCC ranges between 4 and 6 mo[19].

At CEUS, the typical enhancement pattern of HCC is hyperenhancement in the arterial phase followed by gradual and mild wash-out in the portal venous and/or late phases[10] (Figure 2). Washout is represented as a relatively hypoechoic aspect compared to healthy liver parenchyma in the later stages of the study with any type of contrast-enhancement in the arterial phase. In general, at CEUS, the presence of the wash-out sign is highly suggestive of malignancy. In HCC, washout begins over 60-90 s after injection of contrast agent, whereas metastases or intrahepatic cholangiocarcinoma usually show a rapid washout (< 60 s) (Table 2) (Figure 3)[20]. Therefore, in CEUS, an observation period of up to approximately 5 min is required to easily visualize the typically subtle and late (> 1 min) washout of HCC (Figure 2).

Noteworthy, a study showed that arterial enhancement patterns of HCC at CEUS are related to the degree of histologic differentiation: moderately differentiated HCC exhibits a classic behavior after contrast agent injection compared to well-differentiated HCC. Extended observation in the portal phase is important for reporting late washout that in HCC occurs more frequently later than in the portal venous phase[21]. As a caveat, well-differentiated HCC may appear iso-enhancing in the portal-venous or late phase[9].

On the other hand, in a study by Tada *et al*[22], 63 of 68 (92.6%) small HCCs (< 3 cm in size) showed a mainly diffuse and homogeneous enhancement in the arterial-phase whereas large HCCs presented a heterogeneous arterial-phase enhancement pattern mainly related to non-enhancing areas of fibrosis, necrosis or internal hemorrhage.

In general, thanks to the real-time nature of CEUS, its high spatial and temporal resolution, the sensitivity of CEUS in the detection of hypervascularization of cirrhotic nodules was found to be higher compared to CT/MRI[23].

Overall, CEUS showed a sensitivity of 88.8%, a specificity of 89.2% and a PPV of 91.3% in the characterization of HCC[24].

Although it is still a matter of debate, several international guidelines are now endorsing the use of CEUS as a first or second-line diagnostic tool for the diagnosis of HCC[12,25]. In 2016, the American College of Radiology included CEUS in its comprehensive Liver Imaging Reporting and Data System (LI-RADS): a unique scoring system for CEUS examinations in patients with increased risk of HCC. A systematic review comparing the cost-effectiveness of CEUS with CT and MRI confirmed that CEUS is cost-effective in the surveillance of patients with liver cirrhosis[11].

Table 3 shows the main recommendations on the use of CEUS in cirrhotic patients according to the World Federation for Ultrasound in Medicine & Biology[26].

CEUS has shown high sensitivity for the evaluation of portal vein patency and in the differential diagnosis between benign and malignant portal vein thrombosis, this latter occurring in cirrhotic patients at various stages[27]. A thrombus showing hypervascularity in the arterial phase, irrespective of the presence of subsequent washout, is deemed to be malignant[10].

CEUS can also be used with valid results in guidance, response and detection of complications of interventional procedures[28] (Figure 4). CEUS may be of help during or after the interventional procedure[29]. Intraprocedural use of CEUS showed a relevant clinical impact, reducing the number of re-treatments and the related costs per patient[30].

Table 2 Imaging enhancement pattern of cirrhotic nodules and malignant focal liver lesions on Contrast-enhanced ultrasound

Lesion	Arterial phase	Portal venous phase	Late phase	Post-vascular phase
RN	Hypo-enhance	Iso-enhance	Iso-enhance	Iso-enhance
DN	Hypo-enhance or partial hyper-enhanced within lesion (early-HCC)	Iso-enhance	Iso-enhance	Iso-enhance
HCC	Hyper-enhance	Hypo-enhance or iso-enhance	Hypo-enhance or iso-enhance[1]	Hypo-enhance (mild and late washout) or iso-enhance[1]
ICC	Rim-enhance or Hyper-enhance with early washout (< 60 seconds)	Hypo-enhance	Hypo-enhance	Hypo-enhance
Metastasis	Rim-enhance or Hyper-enhance with early washout (< 60 seconds)	Hypo-enhance	Hypo-enhance	Hypo-enhance

[1]Well differentiated hepatocellular carcinoma. RN: Regenerative nodules; DN: Dysplastic nodules; HCC: Hepatocellular carcinoma; ICC: Intrahepatic cholangiocarcinoma.

Table 3 Recommendations contrast-enhanced ultrasound in cirrhotic liver

Recommendations	Notes
Characterization FLLs found in patients with liver cirrhosis to establish a diagnosis of malignancy	CT or MR imaging is required for a complete staging
In nodules not suitable for biopsy	When CT or MR are inconclusive
Selection of FLLs with different contrast pattern in a cirrhotic liver to be biopsied	
Monitoring changes in enhancement patterns in FLLs in cirrhotic liver requiring follow-up	
Guiding percutaneous biopsies to increase the diagnostic outcome	To compare to B-mode US

FLLs: Focal liver lesions; CT: Computed tomography; MR: Magnetic resonance; US: Ultrasounds.

The three-dimensional evaluation through the CEUS of the tumor lesion allows more accurate planning and the treatment with locoregional therapies[31,32] (Figure 5).

Intrahepatic cholangiocarcinoma

Intrahepatic peripheral cholangiocarcinoma (ICC) constitutes the second most common primary liver malignant tumor in cirrhotic patients and accounts for 1%–3% of newly developed tumors[32,33]. Differentiating ICC from HCC is of clinical relevance since liver transplantation is contraindicated in patients with ICC given poorly reported outcomes[34].

At CEUS, ICC shows heterogeneous contrast enhancement in the arterial phase with a substantially hypoechoic appearance in the extended portal-venous phase[35]. A rim-like contrast-enhancement has been reported but with a quite variable range (8-51% of cases)[9]. The presence and the quantity of fibrotic tissue and necrotic areas may strongly influence the CEUS appearance of ICC. This latter may present at CEUS overlapping features with HCC[36]. At CEUS, a clue suggestive for ICC is the presence of a wash out occurring earlier than 60 s, whereas HCC usually washes out later on (Figure 6)[37,38]. The same temporal difference in wash-out between HCC and other malignancies, including ICC, is also used by the CEUS LI-RADS lexicon for the diagnosis of ICC[10].

In a multicenter study of 1,006 nodules from 848 patients, the use of CEUS LI-RADS criteria for HCC - namely, arterial phase hyperenhancement and late washout (onset ≥ 60 s after contrast injection) of mild degree - was 98.5% predictive of HCC with no risk of misdiagnosis for pure cholangiocarcinoma[39]. To this purpose, contrast-enhanced CT and MRI may provide useful information due to the different contrast agent kinetic. Microbubbles are essentially blood pool agents and remain confined to the vascular space, whereas iodinated contrast agent and gadolinium chelates are essentially extra-cellular contrast agents and progressively accumulate in the fibrotic spaces of ICC[39].

The presence of both ICC and HCC components in the same lesion can make the lesion even more difficult and biopsy may be eventually needed in equivocal cases.

Metastasis

Metastatic liver deposits are relatively uncommon in the cirrhotic liver. This finding may probably be due to alteration of hemodynamics and the microstructural environment in the liver[40]. In particular, the hepatofugal portal venous flow may prevent neoplastic cells from seeding and flourishing in the liver[41]. Liver metastases from colorectal carcinoma are infrequently reported to spread to the cirrhotic

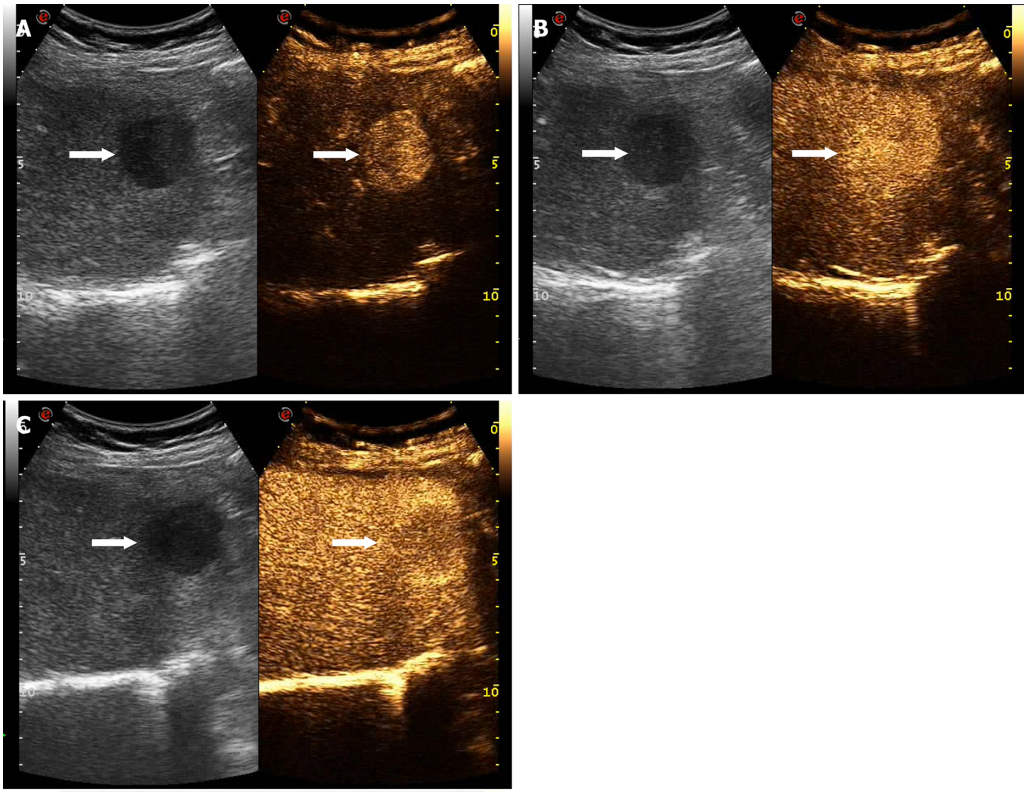

DOI: 10.4329/wjr.v14.i4.70

Figure 2 Hepatocellular carcinoma. A: Contrast-enhanced ultrasound examination in the arterial phase (30 s after the i.v. injection of contrast agent) shows a 3 cm sized hypoechoic nodule, showing a marked contrast enhancement (right, arrow); B: In the portal phase (70 s after the injection) the lesion is still hyper-enhancing in comparison to the adjacent liver parenchyma (arrows); C: Only waiting for the extended portal phase (*i.e.* 122 s after the injection) the lesion shows a mild and late wash-out and appears moderately hypoechoic (arrows).

liver[42]. Metastases from non-Hodgkin B-cell lymphoma may also involve the liver in patients with hepatitis C virus and typically consist of multiple small nodules[43].

On CEUS, liver metastases show a sharp and early washout within 60 s of contrast administration, irrespective of the contrast enhancement type in the arterial phase (Figure 3)[44]. This latter may present various patterns, such as rim-like, dotted, heterogeneous or even homogeneous, depending on the size and the grade of cellularity, vascularity, fibrosis and necrosis accompanying the development of the lesion.

BENIGN LESIONS

A wide spectrum of benign lesions may arise in a cirrhotic liver. Hence, it is crucial to avoid the misdiagnosis of benign liver lesions as HCC (*i.e.* minimize false positives) because this diagnostic interpretation may incorrectly increase the tumor burden[43].

Generally, at CEUS, a benign lesion presents a progressive and sustained enhancement in all phases of the study[45] (Table 4, Figures 7 and 8). Although tumor lesions may have similar characteristics, a clinical context of oncological or cirrhotic pathology allows differentiating the nature of the lesions[21]. Further aspects that are decisive for the diagnosis are detected by observing the arterial phase[4].

Hemangioma

Hemangioma is seen less frequently in cirrhotic patients than in the general population. In general, imaging features remain similar to those of hemangiomas observed in non-cirrhotic patients[46].

At CEUS, hemangioma has a characteristic globular, progressive, peripheral and discontinuous enhancement (Figure 7). However, with progressive cirrhosis, hemangiomas are likely to decrease in size, become more fibrotic and may appear as a hypo vascular lesion with a lack of peripheral globular contrast-enhancement[47,48]. Furthermore, flash filling hemangiomas may pose a diagnostic dilemma with well-differentiated HCC not showing wash-out, thus needing further radiological workup with CT or MRI for the final diagnosis.

Table 4 Imaging enhancement pattern of benign focal liver lesions on contrast-enhanced ultrasound

Lesion	Arterial phase	Portal venous phase	Late phase	Post-vascular phase
Hepatic cysts	Non-enhance	Non-enhance	Non-enhance	Non-enhance
Cystic hydatid disease	Non-enhance cysts and septa	Non-enhance cysts and septa	Non-enhance cysts and septa	Non-enhance cysts and septa
Abscess	Rim-enhance with enhanced septa; no central enhancement	Rim-enhance with enhanced septa; no central enhancement	Hypo-enhance rim; no central enhancement	Hypo-enhance rim; no central enhancement
Hemangioma	Peripheral, discontinuous and globular hyper-enhance	Peripheral, globular iso enhance and fill-in	Iso-enhance or hypo-enhance	Iso-enhance or hypo-enhance
FNH	Hyper-enhance from the center to peripheral region spoke-wheel vascularity	Hyper-enhance with/without un-enhanced central scar	Iso-enhance or hyper-enhance with/without un-enhanced central scar	Iso-enhance or hypo-enhance
HA	Hyper-enhance	Iso-enhance	Iso-enhance	Iso-enhance or hypo-enhance
Pseudo lesions	Hyper-enhance	Hyper-enhance or iso-enhance	Iso-enhance	Iso-enhance

FNH: Focal nodular hyperplasia; HA: Hepatocellular adenoma.

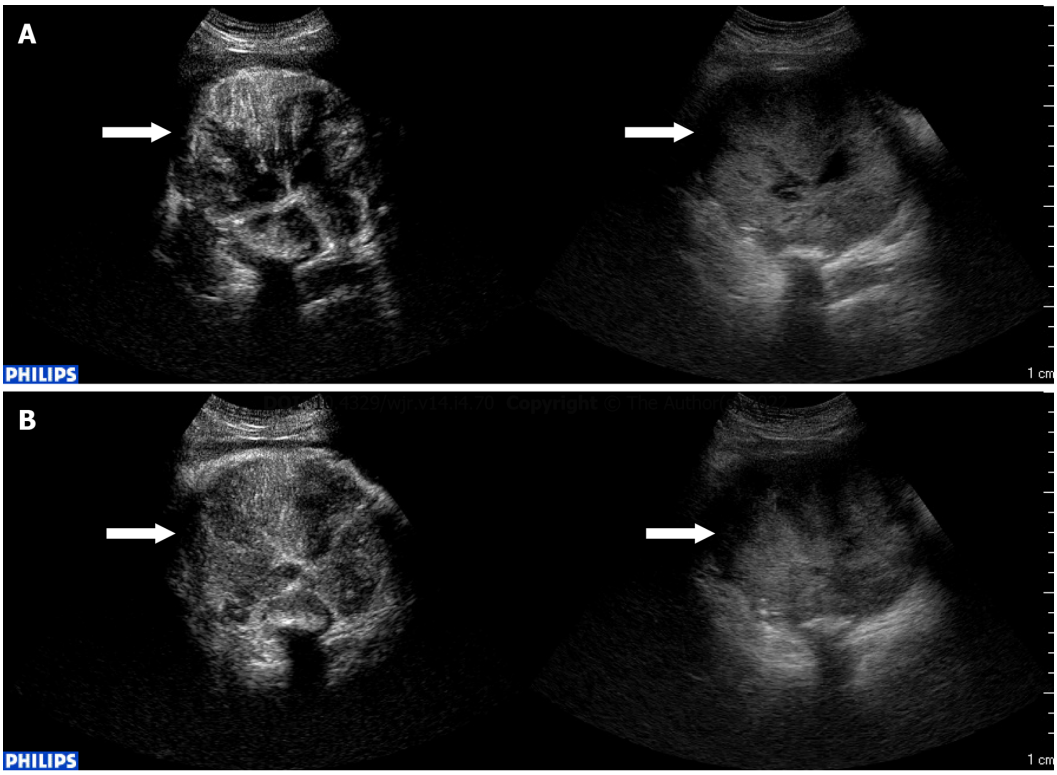

DOI: 10.4329/wjr.v14.i4.70

Figure 3 Liver metastasis from gastrointestinal stromal tumor. A: Contrast-enhanced ultrasound examination in the arterial phase (10 s after the i.v. injection of contrast agent) shows a large (11 cm) mass, showing heterogeneous contrast enhancement (left, arrow); B: Still in the arterial phase (40 s after the injection) the mass shows early wash-out.

Focal nodular hyperplasia

Although Focal nodular hyperplasia (FNH) is the second most common benign liver tumor after hemangioma, the report of FNH-like nodules in the cirrhotic liver is only sporadic and imaging appearance is similar to FNH arising in the non-cirrhotic liver[43,49].

At CEUS, the typical findings of FNH are a centrifugal contrast-enhancement pattern with a spoke-wheel appearance in the arterial phase followed by sustained contrast-enhancement and iso or hyperechoic appearance in portal-venous and late phase[50] (Figure 8). A central avascular area in the arterial phase is often appreciable in FNH larger than 3 cm with a hypoechoic appearance.

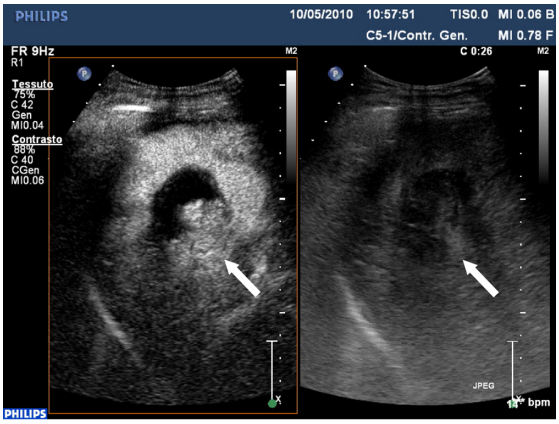

DOI: 10.4329/wjr.v14.i4.70

Figure 4 One-month post-procedural assessment of hepatocellular carcinoma after TACE. Contrast-enhanced ultrasound examination in the arterial phase (26 s after the i.v. injection of contrast agent) shows a clear cut intralesional area of contrast-enhancement indicating still viable tumor.

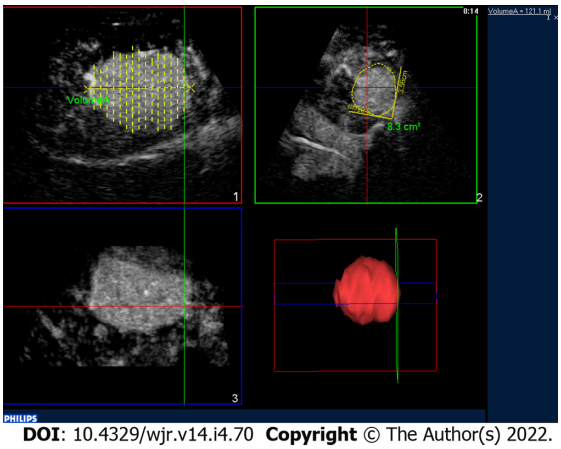

DOI: 10.4329/wjr.v14.i4.70

Figure 5 Contrast-enhanced ultrasound 3D. Contrast-enhanced ultrasound of a hepatocellular carcinoma in the arterial phase: Three-dimensional rendering and volume calculation.

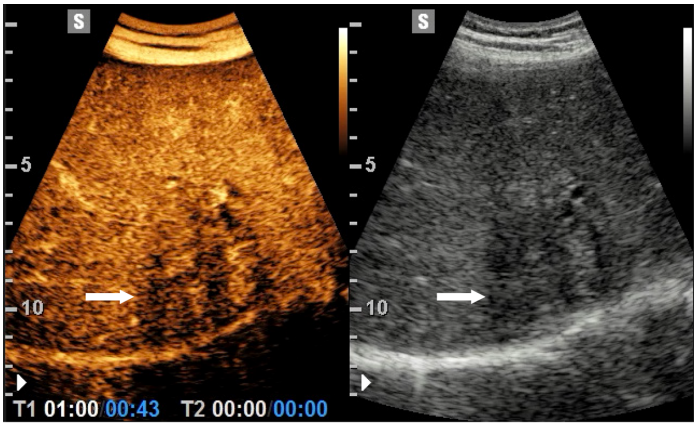

DOI: 10.4329/wjr.v14.i4.70

Figure 6 Intrahepatic cholangiocarcinoma. Contrast-enhanced ultrasound examination in the arterial phase (43 s after the i.v. injection of contrast agent) shows an ill-defined lesion showing heterogeneous washout (left, arrow).

Hepatocellular adenoma

The incidence of hepatocellular adenoma (HA) in the cirrhotic liver is exceedingly rare with a few reports in the literature[51].

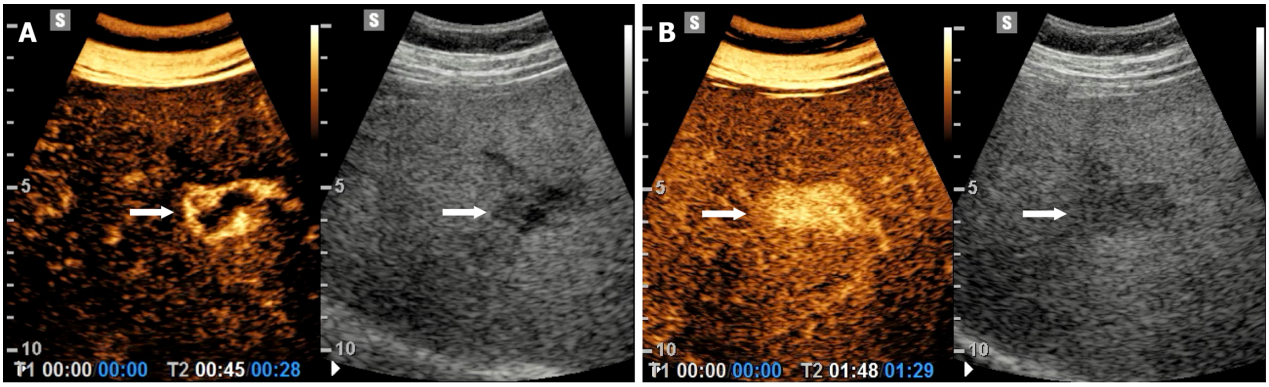

DOI: 10.4329/wjr.v14.i4.70

Figure 7 Hemangioma. A: Contrast-enhanced ultrasound examination in the arterial phase (28 s after the i.v. injection of contrast agent) shows a peripheral globular contrast-enhancement pattern (left, arrow); B: In the portal venous phase (89 s after the injection) a centripetal and complete fill-in is appreciable.

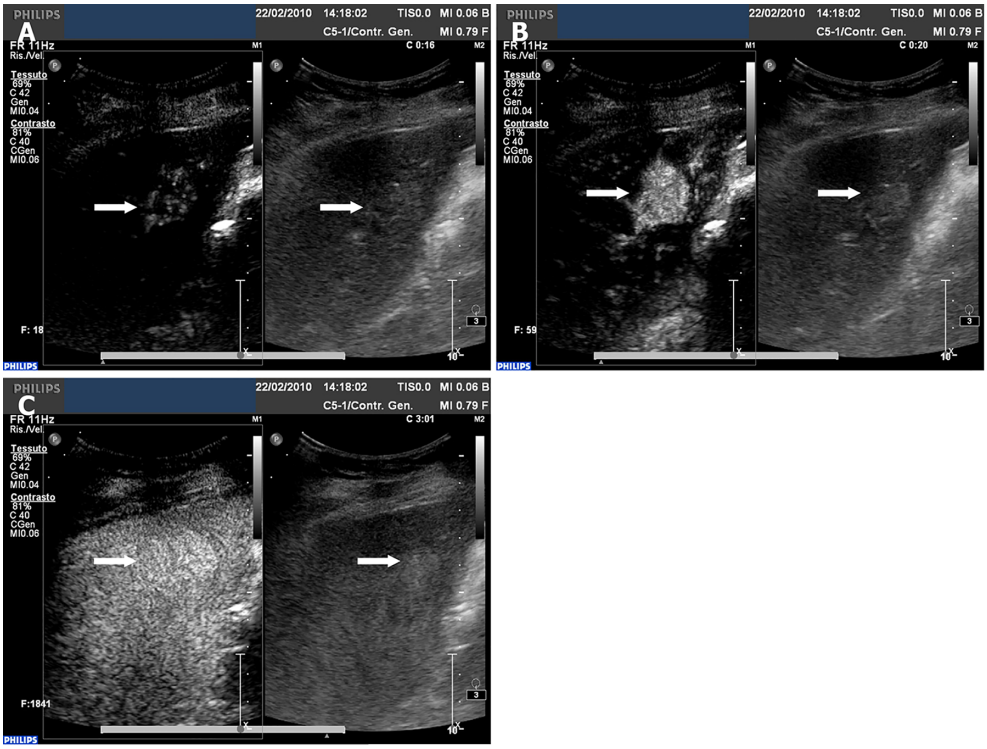

DOI: 10.4329/wjr.v14.i4.70

Figure 8 Focal nodular hyperplasia. A: Contrast-enhanced ultrasound examination in the early arterial phase (16 s after the i.v. injection of contrast agent) shows a spoke-wheel appearance (left, arrow); B: Four seconds later, still in the arterial phase the lesion is homogeneously and strongly enhancing (left, arrow); C: In the late phase (180 s after the injection) the lesion is still slightly hyperechoic to the adjacent liver parenchyma.

At CEUS, a peripheral enhancement with centripetal filling and sustained hypervascularization, suggests the diagnosis of HA[10,52]. However, as a warning, HA may show a hypoechoic appearance in the portal-venous and late phase[52].

Cystic lesions

Simple biliary and peribiliary cysts have similar features in cirrhotic and noncirrhotic livers. They present a homogenous anechoic appearance, a very thin wall and through transmission with posterior acoustic enhancement and no contrast enhancement at CEUS[43]. CEUS may be a problem-solving technique in diagnosing complicated non-anechoic cyst or a rare form of *Co*-existence of hepatocellular carcinoma and cystic echinococcosis[53]. Usually, CEUS shows a lack of enhancement of septa separating daughter cysts[54].

Hepatic abscesses, pyogenic, fungal and amebic have similar CEUS features in cirrhotic and non-cirrhotic livers. Abscesses do not have a significant internal enhancement after contrast ultrasound administration but septations within the lesion may enhance as well as an irregular peripheral rim[55].

Pseudo lesions

Focal fatty changes or confluent hepatic fibrosis can mimic malignancies. Focal fatty changes are an increase or decrease in fat content in a focal area of the liver parenchyma owing to an aberrant portal-venous vascularization[55].

Confluent hepatic fibrosis is usually shown in patients with alcohol-related cirrhosis. It involves peripheral parenchymal replacement by thick fibrotic bands that appear as focal wedge-shaped areas with thick fibrotic bands causing retraction of the overlying capsule; the presence of inflammation can lead to inhomogeneous arterial phase hyperenhancement[40].

At CEUS, these pseudo lesions present isoenhanced in comparison with the surrounding liver parenchyma during the extended portal-venous phase[55], furthermore, fibrosis is usually seen in a typical position (medial segment of the left lobe or anterior segment of the right lobe)[40].

CONCLUSION

A wide spectrum of benign and malignant lesions other than HCC may be found in the cirrhotic liver. More than several years after its release, CEUS is being used for safe diagnostic imaging which enables real-time recognition of enhancement characteristics of focal liver lesions arising in cirrhotic patients. Currently, CEUS is increasingly being performed on a routine basis and is included as a part of the recommended diagnostic work-up of HCC as well as in the follow-up.

FOOTNOTES

Author contributions: Bartolotta TV, Randazzo A, Bruno E and Taibbi A contributed equally to this work; All authors have read and approved the final manuscript.

Conflict-of-interest statement: Tommaso Vincenzo Bartolotta: Lecturer for Samsung.

Country/Territory of origin: Italy

ORCID number: Tommaso Vincenzo Bartolotta 0000-0002-8808-379X; Angelo Randazzo 0000-0001-9558-5248; Eleonora Bruno 0000-0001-6876-2587; Adele Taibbi 0000-0001-6442-744X.

S-Editor: Wang LL
L-Editor: Filipodia
P-Editor: Wang LL

REFERENCES

1 **Tsochatzis EA**, Bosch J, Burroughs AK. Liver cirrhosis. *Lancet* 2014; **383**: 1749-1761 [PMID: 24480518 DOI: 10.1016/S0140-6736(14)60121-5]
2 **Blachier M**, Leleu H, Peck-Radosavljevic M, Valla DC, Roudot-Thoraval F. The burden of liver disease in Europe: a review of available epidemiological data. *J Hepatol* 2013; **58**: 593-608 [PMID: 23419824 DOI: 10.1016/j.jhep.2012.12.005]
3 **Taibbi A**, Petta S, Matranga D, Caruana G, Cannella R, Busè G, Marco VD, Midiri M, Bartolotta TV. Liver stiffness quantification in biopsyproven nonalcoholic fatty liver disease patients using shear wave elastography in comparison with transient elastography. *Ultrasonography* 2020; **40**: 407-416 [PMID: 33561928 DOI: 10.14366/usg.20147]
4 **Ronot M**, Dioguardi Burgio M, Purcell Y, Pommier R, Brancatelli G, Vilgrain V. Focal lesions in cirrhosis: Not always HCC. *Eur J Radiol* 2017; **93**: 157-168 [PMID: 28668410 DOI: 10.1016/j.ejrad.2017.05.040]
5 **Kim MJ**, Lee S, An C. Problematic lesions in cirrhotic liver mimicking hepatocellular carcinoma. *Eur Radiol* 2019; **29**: 5101-5110 [PMID: 30788586 DOI: 10.1007/s00330-019-06030-0]
6 **Quaia E**. Microbubble ultrasound contrast agents: an update. *Eur Radiol* 2007; **17**: 1995-2008 [PMID: 17351779 DOI: 10.1007/s00330-007-0623-0]
7 **Barr RG**, Huang P, Luo Y, Xie X, Zheng R, Yan K, Jing X, Xu H, Fei X, Lee JM. Contrast-enhanced ultrasound imaging of the liver: a review of the clinical evidence for SonoVue and Sonazoid. *Abdom Radiol (NY)* 2020; **45**: 3779-3788 [PMID: 32424608 DOI: 10.1007/s00261-020-02573-9]
8 **Piscaglia F**, Bolondi L; Italian Society for Ultrasound in Medicine and Biology (SIUMB) Study Group on Ultrasound

Contrast Agents. The safety of Sonovue in abdominal applications: retrospective analysis of 23188 investigations. *Ultrasound Med Biol* 2006; **32**: 1369-1375 [PMID: 16965977 DOI: 10.1016/j.ultrasmedbio.2006.05.031]

9 **Durot I**, Wilson SR, Willmann JK. Contrast-enhanced ultrasound of malignant liver lesions. *Abdom Radiol (NY)* 2018; **43**: 819-847 [PMID: 29094174 DOI: 10.1007/s00261-017-1360-8]

10 **Bartolotta TV**, Vernuccio F, Taibbi A, Lagalla R. Contrast-Enhanced Ultrasound in Focal Liver Lesions: Where Do We Stand? *Semin Ultrasound CT MR* 2016; **37**: 573-586 [PMID: 27986175 DOI: 10.1053/j.sult.2016.10.003]

11 **Westwood M**, Joore M, Grutters J, Redekop K, Armstrong N, Lee K, Gloy V, Raatz H, Misso K, Severens J, Kleijnen J. Contrast-enhanced ultrasound using SonoVue® (sulphur hexafluoride microbubbles) compared with contrast-enhanced computed tomography and contrast-enhanced magnetic resonance imaging for the characterisation of focal liver lesions and detection of liver metastases: a systematic review and cost-effectiveness analysis. *Health Technol Assess* 2013; **17**: 1-243 [PMID: 23611316 DOI: 10.3310/hta17160]

12 **Cassinotto C**, Aubé C, Dohan A. Diagnosis of hepatocellular carcinoma: An update on international guidelines. *Diagn Interv Imaging* 2017; **98**: 379-391 [PMID: 28395852 DOI: 10.1016/j.diii.2017.01.014]

13 **Forner A**, Llovet JM, Bruix J. Hepatocellular carcinoma. *Lancet* 2012; **379**: 1245-1255 [PMID: 22353262 DOI: 10.1016/S0140-6736(11)61347-0]

14 **Choi JY**, Lee JM, Sirlin CB. CT and MR imaging diagnosis and staging of hepatocellular carcinoma: part I. Development, growth, and spread: key pathologic and imaging aspects. *Radiology* 2014; **272**: 635-654 [PMID: 25153274 DOI: 10.1148/radiol.14132361]

15 **Kim TK**, Lee KH, Khalili K, Jang HJ. Hepatocellular nodules in liver cirrhosis: contrast-enhanced ultrasound. *Abdom Imaging* 2011; **36**: 244-263 [PMID: 21253723 DOI: 10.1007/s00261-011-9686-0]

16 **Wu W**, Chen M, Yan K, Dai Y, Yin S, Yang W, Fan Z. Evaluation of contrast-enhanced ultrasound for diagnosis of dysplastic nodules with a focus of hepatocellular carcinoma in liver cirrhosis patients. *Chin J Cancer Res* 2015; **27**: 83-89 [PMID: 25717230 DOI: 10.3978/j.issn.1000-9604.2015.02.06]

17 **Ferlay J**, Soerjomataram I, Dikshit R, Eser S, Mathers C, Rebelo M, Parkin DM, Forman D, Bray F. Cancer incidence and mortality worldwide: sources, methods and major patterns in GLOBOCAN 2012. *Int J Cancer* 2015; **136**: E359-E386 [PMID: 25220842 DOI: 10.1002/ijc.29210]

18 **Sato T**, Kondo F, Ebara M, Sugiura N, Okabe S, Sunaga M, Yoshikawa M, Suzuki E, Ogasawara S, Shinozaki Y, Ooka Y, Chiba T, Kanai F, Kishimoto T, Nakatani Y, Fukusato T, Yokosuka O. Natural history of large regenerative nodules and dysplastic nodules in liver cirrhosis: 28-year follow-up study. *Hepatol Int* 2015; **9**: 330-336 [PMID: 25788204 DOI: 10.1007/s12072-015-9620-6]

19 **An C**, Choi YA, Choi D, Paik YH, Ahn SH, Kim MJ, Paik SW, Han KH, Park MS. Growth rate of early-stage hepatocellular carcinoma in patients with chronic liver disease. *Clin Mol Hepatol* 2015; **21**: 279-286 [PMID: 26523271 DOI: 10.3350/cmh.2015.21.3.279]

20 **Bhayana D**, Kim TK, Jang HJ, Burns PN, Wilson SR. Hypervascular liver masses on contrast-enhanced ultrasound: the importance of washout. *AJR Am J Roentgenol* 2010; **194**: 977-983 [PMID: 20308500 DOI: 10.2214/AJR.09.3375]

21 **Jang HJ**, Kim TK, Burns PN, Wilson SR. Enhancement patterns of hepatocellular carcinoma at contrast-enhanced US: comparison with histologic differentiation. *Radiology* 2007; **244**: 898-906 [PMID: 17709836 DOI: 10.1148/radiol.2443061520]

22 **Tada T**, Kumada T, Toyoda H, Ito T, Sone Y, Kaneoka Y, Maeda A, Okuda S, Otobe K, Takahashi K. Utility of Contrast-enhanced Ultrasonography with Perflubutane for Determining Histologic Grade in Hepatocellular Carcinoma. *Ultrasound Med Biol* 2015; **41**: 3070-3078 [PMID: 26360976 DOI: 10.1016/j.ultrasmedbio.2015.07.023]

23 **Maruyama H**, Takahashi M, Ishibashi H, Yoshikawa M, Yokosuka O. Contrast-enhanced ultrasound for characterization of hepatic lesions appearing non-hypervascular on CT in chronic liver diseases. *Br J Radiol* 2012; **85**: 351-357 [PMID: 21224305 DOI: 10.1259/bjr/20440141]

24 **Zheng SG**, Xu HX, Liu LN. Management of hepatocellular carcinoma: The role of contrast-enhanced ultrasound. *World J Radiol* 2014; **6**: 7-14 [PMID: 24578787 DOI: 10.4329/wjr.v6.i1.7]

25 **Kang HJ**, Lee JM, Yoon JH, Han JK. Role of Contrast-Enhanced Ultrasound as a Second-Line Diagnostic Modality in Noninvasive Diagnostic Algorithms for Hepatocellular Carcinoma. *Korean J Radiol* 2021; **22**: 354-365 [PMID: 33236540 DOI: 10.3348/kjr.2020.0973]

26 **Dietrich CF**, Nolsøe CP, Barr RG, Berzigotti A, Burns PN, Cantisani V, Chammas MC, Chaubal N, Choi BI, Clevert DA, Cui X, Dong Y, D'Onofrio M, Fowlkes JB, Gilja OH, Huang P, Ignee A, Jenssen C, Kono Y, Kudo M, Lassau N, Lee WJ, Lee JY, Liang P, Lim A, Lyshchik A, Meloni MF, Correas JM, Minami Y, Moriyasu F, Nicolau C, Piscaglia F, Saftoiu A, Sidhu PS, Sporea I, Torzilli G, Xie X, Zheng R. Guidelines and Good Clinical Practice Recommendations for Contrast-Enhanced Ultrasound (CEUS) in the Liver-Update 2020 WFUMB in Cooperation with EFSUMB, AFSUMB, AIUM, and FLAUS. *Ultrasound Med Biol* 2020; **46**: 2579-2604 [PMID: 32713788 DOI: 10.1016/j.ultrasmedbio.2020.04.030]

27 **Tarantino L**, Ambrosino P, Di Minno MN. Contrast-enhanced ultrasound in differentiating malignant from benign portal vein thrombosis in hepatocellular carcinoma. *World J Gastroenterol* 2015; **21**: 9457-9460 [PMID: 26327753 DOI: 10.3748/wjg.v21.i32.9457]

28 **Francica G**, Meloni MF, Riccardi L, Giangregorio F, Caturelli E, Terracciano F, de Sio I. Role of Contrast-Enhanced Ultrasound in the Detection of Complications After Ultrasound-Guided Liver Interventional Procedures. *J Ultrasound Med* 2020; **40**: 1665-1673 [PMID: 33085814 DOI: 10.1002/jum.15540]

29 **Ferraioli G**, Meloni MF. Contrast-enhanced ultrasonography of the liver using SonoVue. *Ultrasonography* 2018; **37**: 25-35 [PMID: 28830058 DOI: 10.14366/usg.17037]

30 **Mauri G**, Porazzi E, Cova L, Restelli U, Tondolo T, Bonfanti M, Cerri A, Ierace T, Croce D, Solbiati L. Intraprocedural contrast-enhanced ultrasound (CEUS) in liver percutaneous radiofrequency ablation: clinical impact and health technology assessment. *Insights Imaging* 2014; **5**: 209-216 [PMID: 24563244 DOI: 10.1007/s13244-014-0315-7]

31 **Bartolotta TV**, Taibbi A, Matranga D, Midiri M, Lagalla R. 3D vs 2D contrast-enhanced sonography in the evaluation of therapeutic response of hepatocellular carcinoma after locoregional therapies: preliminary findings. *Radiol Med* 2015; **120**: 695-704 [DOI: 10.1007/s11547-015-0514-4]

32 **Rimola J**, Forner A, Tremosini S, Reig M, Vilana R, Bianchi L, Rodríguez-Lope C, Solé M, Ayuso C, Bruix J. Non-invasive diagnosis of hepatocellular carcinoma ≤ 2 cm in cirrhosis. Diagnostic accuracy assessing fat, capsule and signal intensity at dynamic MRI. *J Hepatol* 2012; **56**: 1317-1323 [PMID: 22314420 DOI: 10.1016/j.jhep.2012.01.004]

33 **Sersté T**, Barrau V, Ozenne V, Vullierme MP, Bedossa P, Farges O, Valla DC, Vilgrain V, Paradis V, Degos F. Accuracy and disagreement of computed tomography and magnetic resonance imaging for the diagnosis of small hepatocellular carcinoma and dysplastic nodules: role of biopsy. *Hepatology* 2012; **55**: 800-806 [PMID: 22006503 DOI: 10.1002/hep.24746]

34 **Sapisochín G**, Fernández de Sevilla E, Echeverri J, Charco R. Liver transplantation for cholangiocarcinoma: Current status and new insights. *World J Hepatol* 2015; **7**: 2396-2403 [PMID: 26464755 DOI: 10.4254/wjh.v7.i22.2396]

35 **Loria F**, Loria G, Basile S, Crea G, Frosina L, Di Carlo I. Contrast-enhanced ultrasound appearances of enhancement patterns of intrahepatic cholangiocarcinoma: correlation with pathological findings. *Updates Surg* 2014; **66**: 135-143 [PMID: 24802031 DOI: 10.1007/s13304-014-0251-6]

36 **Vilana R**, Forner A, Bianchi L, García-Criado A, Rimola J, de Lope CR, Reig M, Ayuso C, Brú C, Bruix J. Intrahepatic peripheral cholangiocarcinoma in cirrhosis patients may display a vascular pattern similar to hepatocellular carcinoma on contrast-enhanced ultrasound. *Hepatology* 2010; **51**: 2020-2029 [PMID: 20512990 DOI: 10.1002/hep.23600]

37 **Li R**, Yuan MX, Ma KS, Li XW, Tang CL, Zhang XH, Guo DY, Yan XC. Detailed analysis of temporal features on contrast enhanced ultrasound may help differentiate intrahepatic cholangiocarcinoma from hepatocellular carcinoma in cirrhosis. *PLoS One* 2014; **9**: e98612 [PMID: 24874413 DOI: 10.1371/journal.pone.0098612]

38 **Wildner D**, Bernatik T, Greis C, Seitz K, Neurath MF, Strobel D. CEUS in hepatocellular carcinoma and intrahepatic cholangiocellular carcinoma in 320 patients - early or late washout matters: a subanalysis of the DEGUM multicenter trial. *Ultraschall Med* 2015; **36**: 132-139 [PMID: 25812115 DOI: 10.1055/s-0034-1399147]

39 **Terzi E**, Iavarone M, Pompili M, Veronese L, Cabibbo G, Fraquelli M, Riccardi L, De Bonis L, Sangiovanni A, Leoni S, Zocco MA, Rossi S, Alessi N, Wilson SR, Piscaglia F; CEUS LI-RADS Italy study group collaborators:. Contrast ultrasound LI-RADS LR-5 identifies hepatocellular carcinoma in cirrhosis in a multicenter restropective study of 1,006 nodules. *J Hepatol* 2018; **68**: 485-492 [PMID: 29133247 DOI: 10.1016/j.jhep.2017.11.007]

40 **Elsayes KM**, Chernyak V, Morshid AI, Tang A, Kielar AZ, Bashir MR, Sirlin CB. The spectrum of Pitfalls, Pseudolesions, and Potential Misdiagnoses in Cirrhosis. *AJR Am J Roentgenol* 2018; **211**: 87-96 [PMID: 29932761 DOI: 10.2214/AJR.18.19781]

41 **Seymour K**, Charnley RM. Evidence that metastasis is less common in cirrhotic than normal liver: a systematic review of post-mortem case-control studies. *Br J Surg* 1999; **86**: 1237-1242 [PMID: 10540123 DOI: 10.1046/j.1365-2168.1999.01228.x]

42 **Gervaz P**, Pak-art R, Nivatvongs S, Wolff BG, Larson D, Ringel S. Colorectal adenocarcinoma in cirrhotic patients. *J Am Coll Surg* 2003; **196**: 874-879 [PMID: 12788423 DOI: 10.1016/S1072-7515(03)00117-0]

43 **Galia M**, Taibbi A, Marin D, Furlan A, Dioguardi Burgio M, Agnello F, Cabibbo G, Van Beers BE, Bartolotta TV, Midiri M, Lagalla R, Brancatelli G. Focal lesions in cirrhotic liver: what else beyond hepatocellular carcinoma? *Diagn Interv Radiol* 2014; **20**: 222-228 [PMID: 24509186 DOI: 10.5152/dir.2014.13184]

44 **Bartolotta TV**, Taibbi A, Picone D, Anastasi A, Midiri M, Lagalla R. Detection of liver metastases in cancer patients with geographic fatty infiltration of the liver: the added value of contrast-enhanced sonography. *Ultrasonography* 2017; **36**: 160-169 [PMID: 28145108 DOI: 10.14366/usg.16041]

45 **Zarzour JG**, Porter KK, Tchelepi H, Robbin ML. Contrast-enhanced ultrasound of benign liver lesions. *Abdom Radiol (NY)* 2018; **43**: 848-860 [PMID: 29167944 DOI: 10.1007/s00261-017-1402-2]

46 **Duran R**, Ronot M, Di Renzo S, Gregoli B, Van Beers BE, Vilgrain V. Is magnetic resonance imaging of hepatic hemangioma any different in liver fibrosis and cirrhosis compared to normal liver? *Eur J Radiol* 2015; **84**: 816-822 [PMID: 25703650 DOI: 10.1016/j.ejrad.2015.01.016]

47 **Brancatelli G**, Federle MP, Blachar A, Grazioli L. Hemangioma in the cirrhotic liver: diagnosis and natural history. *Radiology* 2001; **219**: 69-74 [PMID: 11274536 DOI: 10.1148/radiology.219.1.r01ap3269]

48 **Wu XF**, Bai XM, Yang W, Sun Y, Wang H, Wu W, Chen MH, Yan K. Differentiation of atypical hepatic hemangioma from liver metastases: Diagnostic performance of a novel type of color contrast enhanced ultrasound. *World J Gastroenterol* 2020; **26**: 960-972 [PMID: 32206006 DOI: 10.3748/wjg.v26.i9.960]

49 **Lee YH**, Kim SH, Cho MY, Shim KY, Kim MS. Focal nodular hyperplasia-like nodules in alcoholic liver cirrhosis: radiologic-pathologic correlation. *AJR Am J Roentgenol* 2007; **188**: W459-W463 [PMID: 17449744 DOI: 10.2214/AJR.05.1998]

50 **Giambelluca D**, Taibbi A, Midiri M, Bartolotta TV. The "spoke wheel" sign in hepatic focal nodular hyperplasia. *Abdom Radiol (NY)* 2019; **44**: 1183-1184 [PMID: 30488100 DOI: 10.1007/s00261-018-1852-1]

51 **Seo JM**, Lee SJ, Kim SH, Park CK, Ha SY. Hepatocellular carcinoma arising from hepatocellular adenoma in a hepatitis B virus-associated cirrhotic liver. *Clin Radiol* 2012; **67**: 329-333 [PMID: 22079485 DOI: 10.1016/j.crad.2011.09.003]

52 **Garcovich M**, Faccia M, Meloni F, Bertolini E, de Sio I, Calabria G, Francica G, Vidili G, Riccardi L, Zocco MA, Ainora ME, Ponziani FR, De Gaetano AM, Gasbarrini A, Rapaccini GL, Pompili M. Contrast-enhanced ultrasound patterns of hepatocellular adenoma: an Italian multicenter experience. *J Ultrasound* 2019; **22**: 157-165 [PMID: 30306412 DOI: 10.1007/s40477-018-0322-5]

53 **Bo R**, Yasen A, Shao Y, Zhang W, Lin R, Jiang T, Wen H, Xiao H, Aji T. Co-existence of hepatocellular carcinoma and cystic echinococcosis. *Infect Agent Cancer* 2020; **15**: 5 [PMID: 32010203 DOI: 10.1186/s13027-020-0275-0]

54 **Pakala T**, Molina M, Wu GY. Hepatic Echinococcal Cysts: A Review. *J Clin Transl Hepatol* 2016; **4**: 39-46 [PMID: 27047771 DOI: 10.14218/JCTH.2015.00036]

55 **Selkoe DJ**, Hardy J. The amyloid hypothesis of Alzheimer's disease at 25 years. *EMBO Mol Med* 2016; **8**: 595-608 [PMID: 27025652 DOI: 10.15252/emmm.201606210]

World Journal of Radiology

Submit a Manuscript: https://www.f6publishing.com

World J Radiol 2022 April 28; 14(4): 82-90

DOI: 10.4329/wjr.v14.i4.82

ISSN 1949-8470 (online)

ORIGINAL ARTICLE

Retrospective Cohort Study

Decreased cross-sectional muscle area in male patients with clear cell renal cell carcinoma and peritumoral collateral vessels

Federico Greco, Bruno Beomonte Zobel, Carlo Augusto Mallio

Specialty type: Radiology, nuclear medicine and medical imaging

Provenance and peer review: Invited article; Externally peer reviewed.

Peer-review model: Single blind

Peer-review report's scientific quality classification

Grade A (Excellent): 0
Grade B (Very good): 0
Grade C (Good): C, C
Grade D (Fair): 0
Grade E (Poor): E

P-Reviewer: Iida H, Japan; Lin X, China; Sato H, Japan

Received: October 24, 2021
Peer-review started: October 24, 2021
First decision: December 10, 2021
Revised: December 15, 2021
Accepted: March 25, 2022
Article in press: March 25, 2022
Published online: April 28, 2022

Federico Greco, Unità Operativa Complessa Diagnostica per Immagini Territoriale Aziendale, Cittadella della Salute Azienda Sanitaria Locale di Lecce, Lecce 73100, Italy

Bruno Beomonte Zobel, Carlo Augusto Mallio, Unit of Diagnostic Imaging, Università Campus Bio-Medico di Roma, Rome 00128, Italy

Corresponding author: Federico Greco, MD, Doctor, Unità Operativa Complessa Diagnostica per Immagini Territoriale Aziendale, Cittadella della Salute Azienda Sanitaria Locale di Lecce, Piazza Filippo Bottazzi, Lecce 73100, Italy. federicogreco@outlook.com

Abstract

BACKGROUND

Sarcopenia is the loss of skeletal muscle mass (SMM) and is a sign of cancer cachexia. Patients with advanced renal cell carcinoma (RCC) may show cachexia.

AIM

To evaluate the amount of SMM in male clear cell RCC (ccRCC) patients with and without collateral vessels.

METHODS

In this study, we included a total of 124 male Caucasian patients divided into two groups: ccRCCa group without collateral vessels (n = 54) and ccRCCp group with collateral vessels (n = 70). Total abdominal muscle area (TAMA) was measured in both groups using a computed tomography imaging-based approach. TAMA measures were also corrected for age in order to rule out age-related effects.

RESULTS

There was a statistically significant difference between the two groups in terms of TAMA ($P < 0.05$) driven by a reduction in patients with peritumoral collateral vessels. The result was confirmed by repeating the analysis with values corrected for age ($P < 0.05$), indicating no age effect on our findings.

CONCLUSION

This study showed a decreased TAMA in ccRCC patients with peritumoral collateral vessels. The presence of peritumoral collateral vessels adjacent to ccRCC might be a fine diagnostic clue to sarcopenia.

Key Words: Cancer cachexia; Body composition; Clear cell renal cell carcinoma;

Collateral vessels; Kidney cancer; Sarcopenia

Core Tip: Clear cell renal cell carcinoma (ccRCC) can be detected with or without peritumoral collateral vessels. These vessels have been defined as enlarged capsular veins, stimulated by tumor-related effects. The presence of peritumoral collateral vessels around ccRCC is a poorly investigated phenomenon, with unclear clinical meaning. Here, we reported a novel association between peritumoral collateral vessels and loss of skeletal muscle in patients with ccRCC. The effect was not influenced by age, supporting the concept that peritumoral collateral vessels adjacent to ccRCC should drive clinicians' attention towards cancer cachexia.

Citation: Greco F, Beomonte Zobel B, Mallio CA. Decreased cross-sectional muscle area in male patients with clear cell renal cell carcinoma and peritumoral collateral vessels. *World J Radiol* 2022; 14(4): 82-90
URL: https://www.wjgnet.com/1949-8470/full/v14/i4/82.htm
DOI: https://dx.doi.org/10.4329/wjr.v14.i4.82

INTRODUCTION

Cancer cachexia is the reduction of adipose tissue and skeletal muscle (SM) which cannot be fully compensated with nutrition, resulting in progressive functional impairment[1]. This condition is due to energy disbalance during growth of the neoplasm[2]. Advanced neoplastic diseases can lead to loss of up to 85% of adipose and SM tissues[3]. Cancer cachexia and weight loss influence prognosis and response to therapy[4,5]. Renal cell carcinoma (RCC) patients with an advanced and metastatic disease are susceptible to cachexia. RCC patients have a relatively high prevalence of sarcopenia, the term for loss of SM mass (SMM)[4,6]. For example, sarcopenia was detected in up to 47% of patients with localised RCC and 29%-68% of patients with metastatic RCC[7-9]. Sarcopenic RCC patients have a worse overall survival than RCC patients without sarcopenia[10].

SM is not only part of the locomotor system but also produces and releases cytokines and myokines through the contraction of muscle fibres and thus has endocrine activity[11]. By releasing myokines into the circulation, SM can communicate with other organs such as adipose tissue, bone, the liver, and the brain, underlining the importance of this organ for regulating endocrine balance and decreasing risk of various diseases[12].

Body mass index (BMI) is an indicator used for obesity classification but does not convey information about body composition nor does it provide details about the quantity and distribution of different tissues such as SM and abdominal adipose tissue compartments. For this, computed tomography (CT) and magnetic resonance imaging (MRI) are gold standard methods for quantitative assessment and non-invasive tissue characterisation[13-19].

Peritumoural collateral vessels in RCC result from enlargement of capsular renal veins[19]. Gonadal vein recruitment can be present, especially in RCCs located at the lower renal pole[19]. Conversely, lesions located at the upper renal pole have different drainage routes including the adrenal and lower phrenic veins[19]. A study performed on 58 RCC patients reported 28 patients with peritumoural collateral vessels, of which 18 presented with gonadal vein recruitment[19]. Peritumoural collateral vessels with gonadal vein outflow were detected only in RCCs greater than 5 cm in diameter[19].

It is reasonable to speculate that increased blood demand due to tumour hypercellularity and neovascularisation, in possible association with main renal vein thrombosis, are factors contributing to the development of peritumoural collateral vessels in RCC patients. Hypercellularity could influence changes in cellular architecture leading to alternative routes of venous outflow that can become macroscopically evident as peritumoural collateral vessels with CT and MRI imaging (Figure 1). The presence of collateral vessels adjacent to RCC is considered a sign of locally advanced disease (*i.e.*, pT stage > T3a)[20]. However, these vessels can also be present in early stages of RCC.

The direct comparison of SMM in clear cell RCC (ccRCC) patients with and without peritumoural collateral vessels has not been performed to date. Evaluating the relationship between peritumoural collateral vessels in ccRCC patients and reductions of SMM would be of clinical interest for prognostic implications. We hypothesised that ccRCC patients would have a decreased cross-sectional total abdominal muscle area (TAMA) and peritumoural collateral vessels as a metabolic systemic consequence of locally advanced disease. To address this question, we evaluated SMM in male ccRCC patients with and without peritumoural collateral vessels using a CT imaging-based approach.

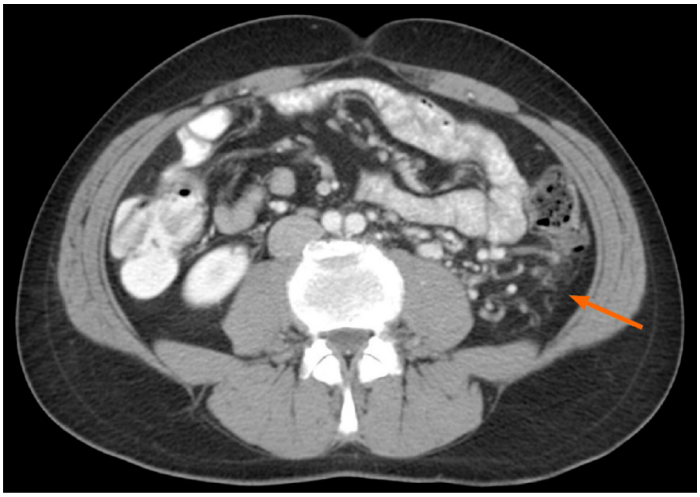

DOI: 10.4329/wjr.v14.i4.82

Figure 1 Axial computed tomography image shows the presence of clear cell renal cell carcinoma collateral vessels with the typical tortuous course located in the retroperitoneal space (arrow).

MATERIALS AND METHODS

This observational retrospective study was conducted in accordance with the Declaration of Helsinki. CT images and data from ccRCC patients with and without peritumoural collateral vessels were downloaded from the Cancer Imaging Archive (TCIA)[21-23]. This data collection received approval from our Institutional Review Board. The subsequent analysis contained publicly available and anonymised data which did not require further review due to previous protections implemented by TCIA. All enrolled subjects signed a written informed consent agreement.

A total of 267 patients with a histologically proven diagnosis of ccRCC were evaluated and selected by examining medical histories and CT images. The exclusion criteria for this study were: Female patients, patients with non-Caucasian ethnicity, patients who had undergone MRI examination only, patients who had undergone chest CT only, heminephrectomised and nephrectomised patients, patients with previous renal ablation, cirrhotic patients with collateral vessels, and patients with a congenital solitary kidney. The selected ccRCC patients were divided into two groups: Absence and presence of collateral vessels (ccRCCa and ccRCCp, respectively).

CT analysis

All ccRCC patients underwent CT examination. Horos v.4.0.0 RC2 software was used for acquisition of TAMA measurements with a semi-automatic function that allowed identification of SM tissue attenuation values (*i.e.*, range 10-40 Hounsfield units)[16]. TAMA (cm^2) was defined as the sum of the areas of the abdominal muscles visible on an axial image located 3 cm above the lower margin of L3 [16]. This area was measured by selecting a region of interest (ROI) on the following muscles: The rectus abdominis, transversus abdominis, external oblique, quadratus lumborum, iliocostalis lumborum, longissimus thoracis, spinalis thoracis, and psoas major[13]. All ROIs were independently drawn by two radiologists (F.G., 5 years of experience; C.A.M., 9 years of experience) who were blinded to the clinical data. The mean of the two measurements was utilised as the value for each subject.

Statistical analysis

Data distribution normality was assessed by the Shapiro-Wilk test. Comparison of TAMA between the ccRCCa and ccRCCp groups was performed using the Student's *t*-test. To rule out age-related effects, TAMA values were corrected by dividing individual values of TAMA by the age of each subject. Sub-analyses for TAMA assessment were performed by Student's *t*-tests between ccRCC patients with low (I/II) or high (III/IV) Fuhrman grade and between patients that were alive or deceased at the time of data collection. To evaluate the reliability of measurements by the two radiologists, the intraclass correlation coefficient for the TAMA measurements was calculated using Cronbach's alpha (also known as coefficient alpha). Finally, Kaplan-Meier curves were included to assess survival of the ccRCCa and ccRCCp groups. The threshold of statistical significance was established at $P < 0.05$.

RESULTS

A total of 124 male Caucasian ccRCC patients were selected according to the exclusion criteria. The two groups were composed as follows: ccRCCa (n = 54; mean age: 57, range: 26-83) and ccRCCp (n = 70; mean age: 59.8, range: 34-84). The staging of ccRCCa group patients were as follows: 1 T1N0M0, 8 T1aN0M0, 21 T1aNxM0, 6 T1bN0M0, 7 T1bNxM0, 1 T1bNxM1, 3 T2N0M0, 1 T2NxM0, 2 T3aN0M0, 2 T3aN0M1, 1 T3bN0M0, and 1 T3bNxM0. The staging of ccRCCp group patients were as follows: 10 T1aNxM0, 1 T1aNxM0, 1 T1aN1M0, 2 T1bN0M0, 8 T1bNxM0, 5 T2N0M0, 1 T2N0M1, 4 T2NxM0, 2 T2aNxM0, 1 T2bN0M0, 9 T3aN0M0, 1 T3aN0M1, 5 T3aNxM0, 1 T3aN0M1, 8 T3aNxM1, 1 T3aN1M1, 3 T3bN0M0, 4 T3bNxM0, 1 T3bNxM1, 1 T4NxM0, and 1 T4N1M1.

Only three (2.41%) of 124 patients had renal vein thrombosis and these three were included in the ccRCCp group (4.28% of ccRCCp patients). No patients had segmental renal vein thrombosis. All patients of the ccRCCp group (n = 70; 100%) showed an exophytic growth pattern. In addition, 31.42% of ccRCCp patients had T1 stage (n = 22), 18.57% T2 (n = 13), 47.14% T3 (n = 33), and 2.85% T4 (n = 2). A total of 28 patients had a history of previous malignancy and 11 patients received a neoadjuvant treatment.

No significant difference was detected in the ages of the two groups (P = 0.21). A statistically significant difference between the ccRCCa and ccRCCp groups was obtained for TAMA (P < 0.05). These results are summarised in Table 1 and represented in Figure 2. Examples of CT cases showing the observed effect are shown in Figure 3. Statistically significant differences between the ccRCCa and ccRCCp groups were confirmed after TAMA values were corrected for age (P < 0.05) (Table 1).

No statistically significant differences (P = 0.66) were found between ccRCC patients with low (n = 44; 1 grade I and 43 grade II) and high (n = 80; 61 grade III and 19 grade IV) Fuhrman grades. These results are summarised in Table 2. Patients who were deceased (n = 33) at the time of data collection demonstrated a statistically significant reduction (P < 0.001) of TAMA in comparison to those that were still alive (n = 90) (Table 3). Cronbach's alpha of the two tracers was 0.913, indicating excellent reliability. No significant differences in survival between the two groups (available data for 54 of 54 ccRCCa patients and 69 of 70 ccRCCp patients) were found based on the Kaplan-Meier method (log-rank test: Z = 1.88, P = 0.06) (Figure 4).

DISCUSSION

This study showed a significant decrease of SMM in the ccRCCp patient group compared to the ccRCCa group. Although SMM is expected to decrease with age, we did not find a significant difference between the ccRCCa and ccRCCp groups in terms of age. This finding was supported by analysis of age-corrected TAMA values. Since differences in SMM can segregate according to gender and ethnicity, only male Caucasian patients were included in the present study to eliminate these potentially confounding factors[24,25].

It has been hypothesised that contraction of myofibres can affect metabolism by triggering the release of humoral/exercise factors from SM which signal for an increase in glucose demand from distant organs[26]. The concept of humoral factors has been progressively developed since cytokine interleukin 6 (IL-6) was found to increase in response to physical exercise causing both autocrine and endocrine effects[27,28].

The cytokines and other peptides produced, expressed, and secreted by SM are called myokines. This term, suggested by Pederson *et al*[29], derives from the Greek words for "muscle" and "motion" and refers to such molecules that exert an endocrine effect on the human body. The physiological consequences of autocrine and paracrine action of myokines includes regulation of muscle growth and lipid metabolism. For example, the myokines produced during exercise, including IL-6, IL-7, IL-15, irisin, and leukaemia inhibitory factor, determine muscle growth by stimulating protein synthesis and hypertrophy. Conversely, myostatin, a member of the transforming growth factor β (TGF-β) superfamily, causes muscle atrophy[30,31]. Activin A, another member of TGF-β superfamily, reproduces the same action of myostatin on SM[30]. Increased blood levels of activin A is known to reduce muscle strength and has been positively correlated with cachexia in cancer patients[32].

Factors that can distort tumour extension such as peritumoural inflammation or the presence of a secondary pseudocapsule can reduce the effectiveness of CT in distinguishing T1 and T2 stages from T3a[19,33]. Incorrect staging, in fact, was detected in 27 of 94 tumours in a study of RCC patients using cross-sectional imaging[19]. Peritumoural collateral vessels in RCC patients showed a specificity of 94% and positive predictive value of 88% in staging of locally advance disease by cross-sectional CT imaging [19].

In our study, 100% of the patients from the ccRCCp group exhibited an exophytic growth pattern. This novel finding suggests a link between peritumour collateral vessels and the RCC growth pattern. Body composition imaging has gained an important role in the assessment of oncological risk, pathogenesis, and development of RCC[14-17]. CT imaging features of the tumour can also provide indications about the patient's body composition. In the present study, the peritumoural collateral

Table 1 Total abdominal muscle area and total abdominal muscle area corrected for age in the two groups

	TAMA (cm²)	TAMA_C (cm²)
ccRCCa group (mean, range, and SD)	164.02 (91, 233.5 ± 31.86)	3.08 (1.29, 5.83 ± 1.06)
ccRCCp group (mean, range, and standard deviation)	150.91 (76.3, 218.3 ± 30.34)	2.67 (1, 4.67 ± 0.91)
P	0.02	0.02

TAMA: Total abdominal muscle area; TAMA_C: Total abdominal muscle area corrected for age; ccRCC: Clear cell renal cell carcinoma.

Table 2 Total abdominal muscle area of clear cell renal cell carcinoma patients with low Fuhrman grade (I/II) and high Fuhrman grade (III/IV)

	TAMA (cm²)
ccRCC patients with low fuhrman grade (I/II) (mean, range, and standard deviation)	158.27 (83.2-233.5), 35.41
ccRCC patients with high Fuhrman grade (III/IV) (mean, range, and standard deviation)	155.71 (76.3-219.2), 29.44
P	0.66

TAMA: Total abdominal muscle area; ccRCC: Clear cell renal cell carcinoma.

Table 3 Total abdominal muscle area of alive and dead clear cell renal cell carcinoma patients

	TAMA (cm²)
Alive ccRCC patients	162.02
(mean, range, and standard deviation)	91, 233.5 ± 28.42
Dead ccRCC patients	150.91
(mean, range, and standard deviation)	76.3, 219.2 ± 34.84
P	0.0008

TAMA: Total abdominal muscle area; ccRCC: Clear cell renal cell carcinoma.

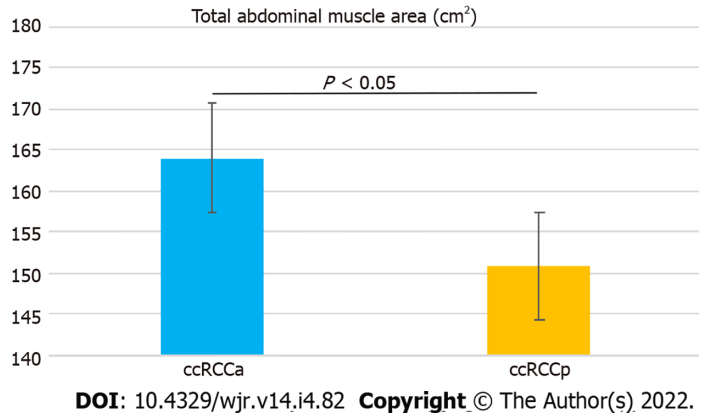

DOI: 10.4329/wjr.v14.i4.82

Figure 2 Bar chart with error bars showing a significant difference in mean values of total abdominal muscle area between the two groups. ccRCC: Clear cell renal cell carcinoma.

vessels adjacent to the ccRCC was associated with a reduction of SMM, a possible sign of sarcopenia. Most likely, in ccRCCp patients, locally advanced disease determines muscle trophism loss as compared to ccRCCa patients. The progressive SMM reduction assessed by CT could be considered a sign of sarcopenia, and therefore of cancer cachexia, with potential prognostic implication for patients. Indeed, deceased ccRCC patients demonstrated a statistically significant reduction of TAMA relative to live

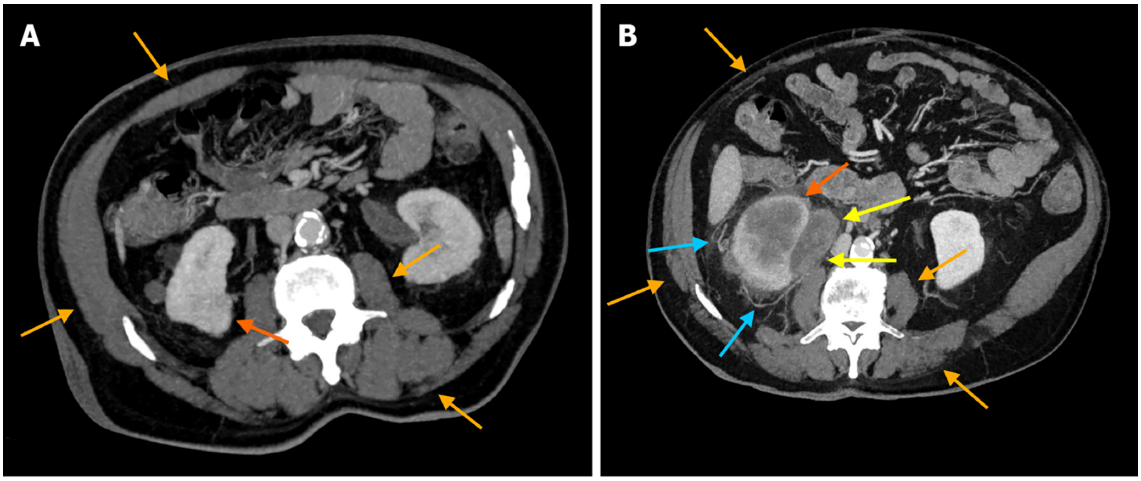

DOI: 10.4329/wjr.v14.i4.82 **Copyright** © The Author(s) 2022.

Figure 3 Axial computed tomography images with maximum intensity projection reconstruction of an 84-year-old male clear cell renal cell carcinoma patient without collateral vessels and an 82-year-old male clear cell renal cell carcinoma patient with collateral vessels. These images show skeletal muscle masses (SMMs) and tumors in a clear cell renal cell carcinoma patient without collateral vessels (ccRCCa) (A) and a clear cell renal cell carcinoma patient with collateral vessels (ccRCCp) (B) (orange and dark orange arrows in A and B, respectively), as well as collateral vessels adjacent to the tumor in the ccRCCp patient (light blue arrows in B) and nodal metastasis infiltrating the ureter (yellow arrows in B). Please note the decrease of SMM clearly evident in the ccRCCp patient (B) compared to the ccRCCa patient (A).

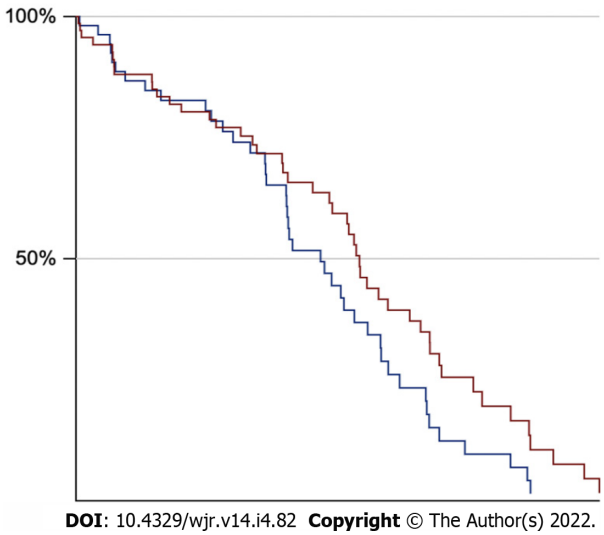

DOI: 10.4329/wjr.v14.i4.82 **Copyright** © The Author(s) 2022.

Figure 4 Kaplan-Meier curves showing no statistically significant difference of survival between the two groups (ccRCCa group is depicted as blue curve and ccRCCb group is depicted as red curve).

patients, suggesting a link between sarcopenia and survival in our sample. However, Kaplan-Maier curves showed a difference just above the statistical threshold between the ccRCCa and ccRCCp patient groups.

The results of this study are supported by recent evidence showing a significant reduction of subcutaneous adipose tissue in ccRCC patients with peritumoural collateral vessels[17]. The limitations of this study include the retrospective study design which did not allow us to assess detailed clinical and anamnestic data including occupation, BMI, hormone blood levels, disease-free survival, timing of CT imaging, performing status, therapies, and CT follow-up after treatment. For instance, testosterone deficiency is known to be associated with an increase in proinflammatory cytokines. Inclusion of hormonal data, such as testosterone levels, could help better understand the cytokine cascade that is associated with pathogenesis and changes in body composition[34,35]. Similarly, CT follow-up after treatment (*e.g.*, surgery or chemotherapy/targeted immunotherapy) would have been helpful to understand changes in the sarcopenia index and the relationship with peritumoural collateral vessels after treatment. The vendor, model, and acquisition parameters (such as slice thickness) of the CT imaging used in this study were also unavailable. Images from the open-source TCIA were often acquired heterogeneously at multiple centres as part of clinical routine. A larger sample size would have

strengthened our multivariate assessment of whether collateral vessels are an independent predictor of sarcopenia as well as the potential impact of other variables such as staging[36-38].

Further studies are needed to evaluate sarcopenia index changes after treatment to add robustness to the role of peritumoural collateral vessels as a prognostic biomarker for ccRCC patients. Such studies should consider abdominal circumference and patients' occupation, which is a factor that can influence SMM (for example, people who are engaged in heavy physical labour would be expected to have significantly more muscle mass compared to office workers)[39]. Finally, SMM content of other subtypes of kidney cancer (*e.g.*, chromophobe and papillary) or other categories of cancer patients should be evaluated to assess the impact of SMM trophism on a patient's health status and prognosis.

CONCLUSION

This study showed a reduction of SMM in ccRCC patients with peritumoural collateral vessels. The presence of peritumoural collateral vessels adjacent to ccRCC is a good candidate biomarker for sarcopenia and therefore of cancer cachexia.

ARTICLE HIGHLIGHTS

Research background

Sarcopenia is the loss of skeletal muscle mass (SMM) and is part of cancer cachexia in which there is a decrease of adipose tissue and SM. Peritumoral collateral vessels adjacent to renal cell carcinoma (RCC) are indicative of locally advanced disease.

Research motivation

Metabolic systemic consequence related to a locally advanced disease might be linked to a decrease of SSM in clear cell RCC (ccRCC) patients with peritumoral collateral vessels, possibly providing clinically relevant information.

Research objectives

The aim of this study was to evaluate the amount of SMM in male ccRCC patients with and without peritumoral collateral vessels, in order to understand a possible relationship between sarcopenia and collateral vessels.

Research methods

In this study, we included a total of 124 male Caucasian patients divided into two groups: ccRCCa (n = 54) and ccRCCp (n = 70) groups, respectively, without and with collateral vessels. Computed tomography imaging-based approach was used for total abdominal muscle area (TAMA) measurements.

Research results

There was a statistically significant difference between the two groups for TAMA ($P < 0.05$).

Research conclusions

This study showed a reduction of TAMA in male ccRCC patients with peritumoral collateral vessels.

Research perspectives

Further studies, on larger sample size and with longitudinal data, will shed light on collateral vessels adjacent to RCC as a possible biomarker of cachexia and sarcopenia.

FOOTNOTES

Author contributions: Greco F and Mallio CA contributed equally to this work; Greco F and Mallio CA designed the research; Greco F and Mallio CA performed the research; Greco F and Mallio CA analyzed the data; Greco F, Beomonte Zobel B, and Mallio CA validated the research; Greco F and Mallio CA wrote the paper; Greco F, Beomonte Zobel B, and Mallio CA supervised the research.

Institutional review board statement: All the procedures were retrospective and agreed with the Declaration of Helsinki. CT images and data of ccRCC patients were retrieved from The Cancer Imaging Archive (TCIA). The TCIA project received approval of the Institutional Review Board. This subsequent retrospective analysis was on the publicly available, anonymized data and did not require further review due to previous protections implemented by

TCIA.

Conflict-of-interest statement: The authors declare that they have no conflict of interest to disclose.

Data sharing statement: The data presented in this study are openly available in The Cancer Imaging Archive (https://wiki.cancerimagingarchive.net/display/Public/TCGA-KIRC, accessed on 1 November 2019).

STROBE statement: The authors have read the STROBE Statement—checklist of items, and the manuscript was prepared and revised according to the STROBE Statement—checklist of items.

Country/Territory of origin: Italy

ORCID number: Federico Greco 0000-0002-9477-0238; Bruno Beomonte Zobel 0000-0001-9227-5535; Carlo Augusto Mallio 0000-0002-0149-0801.

S-Editor: Ma YJ
L-Editor: Wang TQ
P-Editor: Ma YJ

REFERENCES

1 **Tisdale MJ**. Mechanisms of cancer cachexia. *Physiol Rev* 2009; **89**: 381-410 [PMID: 19342610 DOI: 10.1152/physrev.00016.2008]
2 **Daas SI**, Rizeq BR, Nasrallah GK. Adipose tissue dysfunction in cancer cachexia. *J Cell Physiol* 2018; **234**: 13-22 [PMID: 30078199 DOI: 10.1002/jcp.26811]
3 **Murphy RA**, Wilke MS, Perrine M, Pawlowicz M, Mourtzakis M, Lieffers JR, Maneshgar M, Bruera E, Clandinin MT, Baracos VE, Mazurak VC. Loss of adipose tissue and plasma phospholipids: relationship to survival in advanced cancer patients. *Clin Nutr* 2010; **29**: 482-487 [PMID: 19959263 DOI: 10.1016/j.clnu.2009.11.006]
4 **Semeniuk-Wojtaś A**, Lubas A, Stec R, Syryło T, Niemczyk S, Szczylik C. Neutrophil-to-lymphocyte Ratio, Platelet-to-lymphocyte Ratio, and C-reactive Protein as New and Simple Prognostic Factors in Patients With Metastatic Renal Cell Cancer Treated With Tyrosine Kinase Inhibitors: A Systemic Review and Meta-analysis. *Clin Genitourin Cancer* 2018; **16**: e685-e693 [PMID: 29454639 DOI: 10.1016/j.clgc.2018.01.010]
5 **Blum D**, Stene GB, Solheim TS, Fayers P, Hjermstad MJ, Baracos VE, Fearon K, Strasser F, Kaasa S; Euro-Impact. Validation of the Consensus-Definition for Cancer Cachexia and evaluation of a classification model--a study based on data from an international multicentre project (EPCRC-CSA). *Ann Oncol* 2014; **25**: 1635-1642 [PMID: 24562443 DOI: 10.1093/annonc/mdu086]
6 **Martin L**, Birdsell L, Macdonald N, Reiman T, Clandinin MT, McCargar LJ, Murphy R, Ghosh S, Sawyer MB, Baracos VE. Cancer cachexia in the age of obesity: skeletal muscle depletion is a powerful prognostic factor, independent of body mass index. *J Clin Oncol* 2013; **31**: 1539-1547 [PMID: 23530101 DOI: 10.1200/JCO.2012.45.2722]
7 **Psutka SP**, Boorjian SA, Moynagh MR, Schmit GD, Costello BA, Thompson RH, Stewart-Merrill SB, Lohse CM, Cheville JC, Leibovich BC, Tollefson MK. Decreased Skeletal Muscle Mass is Associated with an Increased Risk of Mortality after Radical Nephrectomy for Localized Renal Cell Cancer. *J Urol* 2016; **195**: 270-276 [PMID: 26292038 DOI: 10.1016/j.juro.2015.08.072]
8 **Sharma P**, Zargar-Shoshtari K, Caracciolo JT, Fishman M, Poch MA, Pow-Sang J, Sexton WJ, Spiess PE. Sarcopenia as a predictor of overall survival after cytoreductive nephrectomy for metastatic renal cell carcinoma. *Urol Oncol* 2015; **33**: 339.e17-339.e23 [PMID: 26094169 DOI: 10.1016/j.urolonc.2015.01.011]
9 **Fukushima H**, Nakanishi Y, Kataoka M, Tobisu K, Koga F. Prognostic Significance of Sarcopenia in Patients with Metastatic Renal Cell Carcinoma. *J Urol* 2016; **195**: 26-32 [PMID: 26292042 DOI: 10.1016/j.juro.2015.08.071]
10 **Hu X**, Liao DW, Yang ZQ, Yang WX, Xiong SC, Li X. Sarcopenia predicts prognosis of patients with renal cell carcinoma: A systematic review and meta-analysis. *Int Braz J Urol* 2020; **46**: 705-715 [PMID: 32213202 DOI: 10.1590/S1677-5538.IBJU.2019.0636]
11 **Pedersen BK**. Muscle as a secretory organ. *Compr Physiol* 2013; **3**: 1337-1362 [PMID: 23897689 DOI: 10.1002/cphy.c120033]
12 **Pedersen L**, Hojman P. Muscle-to-organ cross talk mediated by myokines. *Adipocyte* 2012; **1**: 164-167 [PMID: 23700527 DOI: 10.4161/adip.20344]
13 **Prado CM**, Heymsfield SB. Lean tissue imaging: a new era for nutritional assessment and intervention. *JPEN J Parenter Enteral Nutr* 2014; **38**: 940-953 [PMID: 25239112 DOI: 10.1177/0148607114550189]
14 **Greco F**, Mallio CA, Grippo R, Messina L, Vallese S, Rabitti C, Quarta LG, Grasso RF, Beomonte Zobel B. Increased visceral adipose tissue in male patients with non-clear cell renal cell carcinoma. *Radiol Med* 2020; **125**: 538-543 [PMID: 32067162 DOI: 10.1007/s11547-020-01146-6]

15 **Greco F**, Quarta LG, Grasso RF, Beomonte Zobel B, Mallio CA. Increased visceral adipose tissue in clear cell renal cell carcinoma with and without peritumoral collateral vessels. *Br J Radiol* 2020; **93**: 20200334 [PMID: 32516557 DOI: 10.1259/bjr.20200334]

16 **Greco F**, Mallio CA. Relationship between visceral adipose tissue and genetic mutations (VHL and KDM5C) in clear cell renal cell carcinoma. *Radiol Med* 2021; **126**: 645-651 [PMID: 33400184 DOI: 10.1007/s11547-020-01310-y]

17 **Greco F**, Quarta LG, Carnevale A, Giganti M, Grasso RF, Beomonte Zobel B, Mallio CA. Subcutaneous Adipose Tissue Reduction in Patients with Clear Cell Renal Cell Carcinoma and Peritumoral Collateral Vessels: A Retrospective Observational Study. *Appl Sci* 2021; **11**: 6076

18 **Greco F**, Faiella E, Santucci D, Mallio CA, Nezzo M, Quattrocchi CC, Beomonte Zobel B, Grasso RF. Imaging of Renal Medullary Carcinoma. J Kidney Cancer VHL. 2017 4:1-7 [PMID: 28405543 DOI: 10.15586/jkcvhl.2017.62]

19 **Murphy BL**, Gaa J, Papanicolaou N, Lee MJ. Gonadal vein recruitment in renal cell carcinoma: incidence, pathogenesis and clinical significance. *Clin Radiol* 1996; **51**: 797-800 [PMID: 8937323 DOI: 10.1016/s0009-9260(96)80008-0]

20 **Bradley AJ**, MacDonald L, Whiteside S, Johnson RJ, Ramani VA. Accuracy of preoperative CT T staging of renal cell carcinoma: which features predict advanced stage? *Clin Radiol* 2015; **70**: 822-829 [PMID: 25953656 DOI: 10.1016/j.crad.2015.03.013]

21 **NIH National Cancer Institute**. Available from: https://cancergenome.nih.gov/

22 **Akin O**, Elnajjar P, Heller M, Jarosz R, Erickson B, Kirk S, Lineham M, Gautam R, Vikram R, Garcia KM, Roche C, Bonaccio E, Filippini J. Radiology Data from The Cancer Genome Atlas Kidney Renal Clear Cell Carcinoma [TCGA-KIRC] collection. The Cancer Imaging Archive 2016

23 **Clark K**, Vendt B, Smith K, Freymann J, Kirby J, Koppel P, Moore S, Phillips S, Maffitt D, Pringle M, Tarbox L, Prior F. The Cancer Imaging Archive (TCIA): maintaining and operating a public information repository. *J Digit Imaging* 2013; **26**: 1045-1057 [PMID: 23884657 DOI: 10.1007/s10278-013-9622-7]

24 **Janssen I**, Heymsfield SB, Wang ZM, Ross R. Skeletal muscle mass and distribution in 468 men and women aged 18-88 yr. *J Appl Physiol (1985)* 2000; **89**: 81-88 [PMID: 10904038 DOI: 10.1152/jappl.2000.89.1.81]

25 **Silva AM**, Shen W, Heo M, Gallagher D, Wang Z, Sardinha LB, Heymsfield SB. Ethnicity-related skeletal muscle differences across the lifespan. *Am J Hum Biol* 2010; **22**: 76-82 [PMID: 19533617 DOI: 10.1002/ajhb.20956]

26 **Goldstein MS**. Humoral nature of the hypoglycemic factor of muscular work. *Diabetes* 1961; **10**: 232-234 [PMID: 13706674 DOI: 10.2337/diab.10.3.232]

27 **Ostrowski K**, Rohde T, Zacho M, Asp S, Pedersen BK. Evidence that interleukin-6 is produced in human skeletal muscle during prolonged running. *J Physiol* 1998; **508** (Pt 3): 949-953 [PMID: 9518745 DOI: 10.1111/j.1469-7793.1998.949bp.x]

28 **Steensberg A**, van Hall G, Osada T, Sacchetti M, Saltin B, Klarlund Pedersen B. Production of interleukin-6 in contracting human skeletal muscles can account for the exercise-induced increase in plasma interleukin-6. *J Physiol* 2000; **529**: 237-242 [PMID: 11080265 DOI: 10.1111/j.1469-7793.2000.00237.x]

29 **Pedersen BK**, Steensberg A, Fischer C, Keller C, Keller P, Plomgaard P, Febbraio M, Saltin B. Searching for the exercise factor: is IL-6 a candidate? *J Muscle Res Cell Motil* 2003; **24**: 113-119 [PMID: 14609022 DOI: 10.1023/a:1026070911202]

30 **Deshmukh AS**, Cox J, Jensen LJ, Meissner F, Mann M. Secretome Analysis of Lipid-Induced Insulin Resistance in Skeletal Muscle Cells by a Combined Experimental and Bioinformatics Workflow. *J Proteome Res* 2015; **14**: 4885-4895 [PMID: 26457550 DOI: 10.1021/acs.jproteome.5b00720]

31 **Grube L**, Dellen R, Kruse F, Schwender H, Stühler K, Poschmann G. Mining the Secretome of C2C12 Muscle Cells: Data Dependent Experimental Approach To Analyze Protein Secretion Using Label-Free Quantification and Peptide Based Analysis. *J Proteome Res* 2018; **17**: 879-890 [PMID: 29322779 DOI: 10.1021/acs.jproteome.7b00684]

32 **Loumaye A**, de Barsy M, Nachit M, Lause P, Frateur L, van Maanen A, Trefois P, Gruson D, Thissen JP. Role of Activin A and myostatin in human cancer cachexia. *J Clin Endocrinol Metab* 2015; **100**: 2030-2038 [PMID: 25751105 DOI: 10.1210/jc.2014-4318]

33 **Frank I**, Blute ML, Cheville JC, Lohse CM, Weaver AL, Zincke H. An outcome prediction model for patients with clear cell renal cell carcinoma treated with radical nephrectomy based on tumor stage, size, grade and necrosis: the SSIGN score. *J Urol* 2002; **168**: 2395-2400 [PMID: 12441925 DOI: 10.1097/01.ju.0000035885.91935.d5]

34 **Ficarra V**, Galfano A, Mancini M, Martignoni G, Artibani W. TNM staging system for renal-cell carcinoma: current status and future perspectives. *Lancet Oncol* 2007; **8**: 554-558 [PMID: 17540307 DOI: 10.1016/S1470-2045(07)70173-0]

35 **Mohamad NV**, Wong SK, Wan Hasan WN, Jolly JJ, Nur-Farhana MF, Ima-Nirwana S, Chin KY. The relationship between circulating testosterone and inflammatory cytokines in men. *Aging Male* 2019; **22**: 129-140 [PMID: 29925283 DOI: 10.1080/13685538.2018.1482487]

36 **Gu W**, Wu J, Liu X, Zhang H, Shi G, Zhu Y, Ye D. Early skeletal muscle loss during target therapy is a prognostic biomarker in metastatic renal cell carcinoma patients. *Sci Rep* 2017; **7**: 7587 [PMID: 28790354 DOI: 10.1038/s41598-017-07955-6]

37 **Choi Y**, Oh DY, Kim TY, Lee KH, Han SW, Im SA, Bang YJ. Skeletal Muscle Depletion Predicts the Prognosis of Patients with Advanced Pancreatic Cancer Undergoing Palliative Chemotherapy, Independent of Body Mass Index. *PLoS One* 2015; **10**: e0139749 [PMID: 26437072 DOI: 10.1371/journal.pone.0139749]

38 **Sato H**, Goto T, Hayashi A, Kawabata H, Okada T, Takauji S, Sasajima J, Enomoto K, Fujiya M, Oyama K, Ono Y, Sugitani A, Mizukami Y, Okumura T. Prognostic significance of skeletal muscle decrease in unresectable pancreatic cancer: Survival analysis using the Weibull exponential distribution model. *Pancreatology* 2021; **21**: 892-902 [PMID: 33722506 DOI: 10.1016/j.pan.2021.03.002]

39 **Fang H**, Berg E, Cheng X, Shen W. How to best assess abdominal obesity. *Curr Opin Clin Nutr Metab Care* 2018; **21**: 360-365 [PMID: 29916924 DOI: 10.1097/MCO.0000000000000485]

World Journal of Radiology

Submit a Manuscript: https://www.f6publishing.com

World J Radiol 2022 April 28; 14(4): 91-103

DOI: 10.4329/wjr.v14.i4.91

ISSN 1949-8470 (online)

ORIGINAL ARTICLE

Retrospective Study

Outcome of percutaneous drainage for septic complications coexisted with COVID-19

Mohamed A Deif, Ahmad M Mounir, Sherif A Abo-Hedibah, Ahmed M Abdel Khalek, Ali H Elmokadem

Specialty type: Radiology, nuclear medicine and medical imaging

Provenance and peer review: Invited article; Externally peer reviewed.

Peer-review model: Single blind

Peer-review report's scientific quality classification

Grade A (Excellent): 0
Grade B (Very good): B, B
Grade C (Good): 0
Grade D (Fair): 0
Grade E (Poor): 0

P-Reviewer: Wang CY, Taiwan; Wang D, Thailand

Received: December 29, 2021
Peer-review started: December 29, 2021
First decision: February 21, 2022
Revised: March 13, 2022
Accepted: April 9, 2022
Article in press: April 9, 2022
Published online: April 28, 2022

Mohamed A Deif, Department of Radiology, National Liver Institute, Menoufia University, Shibin Al Kawm 32521, Egypt

Ahmad M Mounir, Ahmed M Abdel Khalek, Ali H Elmokadem, Department of Radiology, Mansoura University, Mansoura 35516, Egypt

Sherif A Abo-Hedibah, Department of Radiology, Cairo university, Cairo 12613, Egypt

Corresponding author: Ali H Elmokadem, MD, PhD, Associate Professor, Department of Radiology, Mansoura University, Elgomhoria St, Mansoura 35516, Egypt.
mokadem83@yahoo.com

Abstract

BACKGROUND

The resulting tissue hypoxia and increased inflammation secondary to severe coronavirus disease 2019 (COVID-19) combined with viral load, and other baseline risk factors contribute to an increased risk of severe sepsis or co-existed septic condition exaggeration.

AIM

To describe the clinical, radiological, and laboratory characteristics of a small cohort of patients infected by severe acute respiratory syndrome coronavirus 2 who underwent percutaneous drainage for septic complications and their post-procedural outcomes.

METHODS

This retrospective study consisted of 11 patients who were confirmed to have COVID-19 by RT-PCR test and required drain placement for septic complications. The mean age ± SD of the patients was 48.5 ± 14 years (range 30-72 years). Three patients underwent cholecystostomy for acute acalculous cholecystitis. Percutaneous drainage was performed in seven patients; two peripancreatic collections; two infected leaks after hepatic resection; one recurrent hepatic abscess, one psoas abscess and one lumbar abscess. One patient underwent a percutaneous nephrostomy for acute pyelonephritis.

RESULTS

Technical success was achieved in 100% of patients, while clinical success was achieved in 4 out of 11 patients (36.3%). Six patients (54.5%) died despite proper

percutaneous drainage and adequate antibiotic coverage. One patient (9%) needed operative intervention. Two patients (18.2%) had two drainage procedures to drain multiple fluid collections. Two patients (18.2%) had repeat drainage procedures due to recurrent fluid collections. The average volume of the drained fluid immediately after tube insertion was 85 mL. Follow-up scans show a reduction of the retained content and associated inflammatory changes after tube insertion in all patients. There was no significant statistical difference (P = 0.6 and 0.4) between the mean of WBCs and neutrophils count before drainage and seven days after drainage. The lymphocyte count shows significant increased seven days after drainage (P = 0.03).

CONCLUSION

In this study, patients having septic complications associated with COVID-19 showed relatively poor clinical outcomes despite technically successful percutaneous drainage.

Key Words: COVID-19; SARS-CoV-2; Coronavirus; Sepsis; Drainage; Abscess

Core Tip: This article highlights the relationship between coronavirus disease 2019 (COVID-19) and sepsis. COVID-19 is associated with high risk of severe sepsis or exaggeration of co-existed septic condition. Percutaneous drainage of septic complications co-existed with COVID-19 associated with relatively poor clinical outcomes despite technically successful procedures.

Citation: Deif MA, Mounir AM, Abo-Hedibah SA, Abdel Khalek AM, Elmokadem AH. Outcome of percutaneous drainage for septic complications coexisted with COVID-19. *World J Radiol* 2022; 14(4): 91-103
URL: https://www.wjgnet.com/1949-8470/full/v14/i4/91.htm
DOI: https://dx.doi.org/10.4329/wjr.v14.i4.91

INTRODUCTION

Sepsis is defined as a life-threatening organ dysfunction that happens due to dysregulated host response to an infection[1]. In the bacterial type of sepsis, which is the most frequent etiology, early and rapid therapy by the appropriate antibiotic is essential to reduce the incidence of complications and mortality rates. Most patients infected by severe acute respiratory syndrome coronavirus 2 (SARS-CoV-2) present no severe symptomatology, but almost 5% of patients show severe lung injury or even multiple organ dysfunction syndrome, with mortality at the ICUs between 8% and 38% depending on the country[2,3]. Patients admitted to ICU showed a dysregulated host response in the form of hyperinflammation, changes in the coagulation profile, and dysregulation in the immune response[4], similar to what happens in bacterial sepsis[5,6]. The body's adaptive protection mechanism is formed by a moderate inflammatory response and immune suppression, and if any of them become excessive or uncontrolled, this protective compensation will transform into destructive and decompensated status, then sepsis develops[7-9]. Accordingly, most deaths in critically ill coronavirus disease 2019 (COVID-19) patients are caused by sepsis[10,11].

Hematological examinations for COVID-19 patients show elevated cytokines, C-reactive protein (CRP), abnormal liver and myocardial enzymes decreased lymphocytes, declined platelets, and increased D-dimmer[12]. These findings are similar to sepsis caused by bacterial infections. So, severe COVID-19 could be a sepsis-induced by viral infection causing severe systemic inflammatory response (so-called inflammatory storm)[13,14]. Inflammatory storms are not unique to COVID-19 but also happen in other respiratory viral infections that mimic COVID-19[15,16], such as influenza, SARS, avian influenza, swine flu, and MERS[17-19]. Additionally, specimen cultures in about 80% of COVID-19 patients with septic complications show no bacterial or fungal infection, and the viral infection seems to be the only cause for sepsis[20,21]. Accordingly, sepsis is expected to be responsible for worsening the clinical conditions of these critically ill COVID-19 patients. Our objective was to describe the clinical, radiological, and laboratory characteristics of a small cohort of patients infected by SARS-CoV-2 who underwent percutaneous drainage and their post-procedural outcomes. We hypothesized that septic complication associated with severe COVID-19 has a poor outcome despite adequate percutaneous drainage and antibiotic therapy.

MATERIALS AND METHODS

Patient selection

A local institutional review board approved this retrospective study, and waivers of consent of medical record review were received. COVID-19 patients who underwent image-guided percutaneous drainage for suspected septic complications were identified. Patient demographics and clinical and radiological reports were obtained through electronic medical records and picture archiving and communication system (PACS). The severity of the pulmonary parenchymal involvement and distribution of the pulmonary lesions secondary to COVID-19 was assessed by chest X-ray in 4 patients and chest CT in 7 patients. Flow chart of the study is shown in Figure 1.

Patients demographics

Eleven patients (10 males and 1 female) who were confirmed to have COVID-19 by RT-PCR test required drain placement for septic complications. The mean age ± SD of the patients was 48.5 ± 14 years (range 30-72 years). Three patients underwent cholecystostomy for acute acalculous cholecystitis (Figure 2). Percutaneous drainage was performed in seven patients; two peripancreatic collections (Figure 3); two infected bile leaks in hepatic donor and after resection of hepatic hemangioma; one recurrent hepatic abscess after eight days of surgical evacuation (Figure 4), one psoas abscess (Figure 5) and one lumbar abscess. One patient underwent percutaneous nephrostomy for acute pyelonephritis (Figure 6).

Study outcomes

The primary outcome measures were technical and clinical success. The technical success was achieved by completion of the procedure without procedural complications, while the definition of clinical success was the resolution of symptoms without the subsequent need for operative drainage or patient mortality secondary to related sepsis. Secondary outcomes included the amount of drained fluid, microbial analysis of drained fluid, the period of tube drainage, and changes in laboratory findings before and after drainage.

Percutaneous drainage procedures

Septic complications were diagnosed by ultrasonography, computed tomography, or magnetic resonance imaging. Two interventional radiologists at two institutions with 10 and 13 years of experience performed all percutaneous drainage procedures. All procedures were done after administration of local anesthesia. Percutaneous access into the collections, inflamed gall bladder, or kidney was achieved under sonographic guidance with an 18- or 21-gauge needle. Using the Seldinger technique and micro-puncture set, following serial dilatations, a drainage catheter was placed. The drainage catheters used ranged from 8-French to 10-French. In all cases, no immediate complications were noted.

Antibiotic therapy was started once the symptoms of septic complications presented on the patients. The antibiotics regimen was readjusted according to the drained fluid culture results. The drained fluid for each patient was analyzed regarding its character and maximum possible volume when the tubes were initially placed. Then a fluid sample was sent for bacterial culture and gram stain evaluation. Patients were observed for any major complications requiring surgical intervention till the last date of follow-up.

Statistical analysis

Data were analyzed with SPSS® V. 21 (IBM Corp., New York, NY, United States; formerly SPSS Inc., Chicago, IL, United States). The normality of data was first tested with the Shapiro test. Qualitative data were described using numbers and percentages. Continuous variables were presented as mean ± SD for parametric data and median (range) for non-parametric data. Finally, the laboratory findings were compared with Wilcoxon test.

RESULTS

Fever and abdominal pain were the most common presenting symptoms, and acute kidney injury (AKI) was the most frequent comorbidity. Technical success was achieved in 100% of patients, while clinical success was achieved only in 4 of 11 patients (36.4%). Despite percutaneous drainage, one patient (9%) needed exploratory laparotomy five days after drainage that revealed perforated sigmoid colon, which was managed by resection followed by patient improvement and discharge after 18 d. Six other patients (54.5%) died within a month after proper percutaneous drainage and adequate antibiotic coverage, all of them were admitted to ICU and put under mechanical ventilation. The cause of death was overlapped between COVID-19 related respiratory failure and sepsis. One patient needed cystogasterostomy for peripancreatic collection after 21 d of tube insertion. Two patients (18.2%) had two drainage procedures to drain multiple fluid collections. Two patients (18.2%) had recurrent fluid collections and repeated

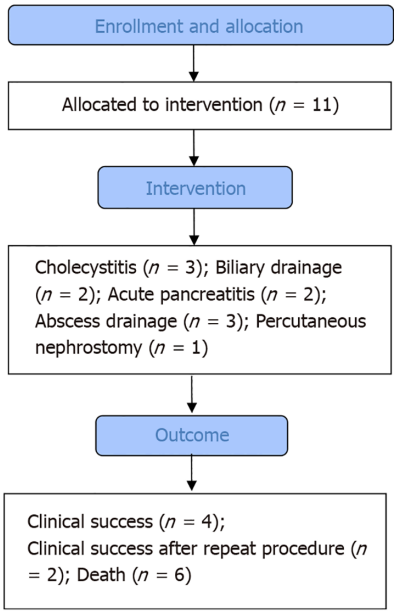

DOI: 10.4329/wjr.v14.i4.91

Figure 1 Flow chart of the study.

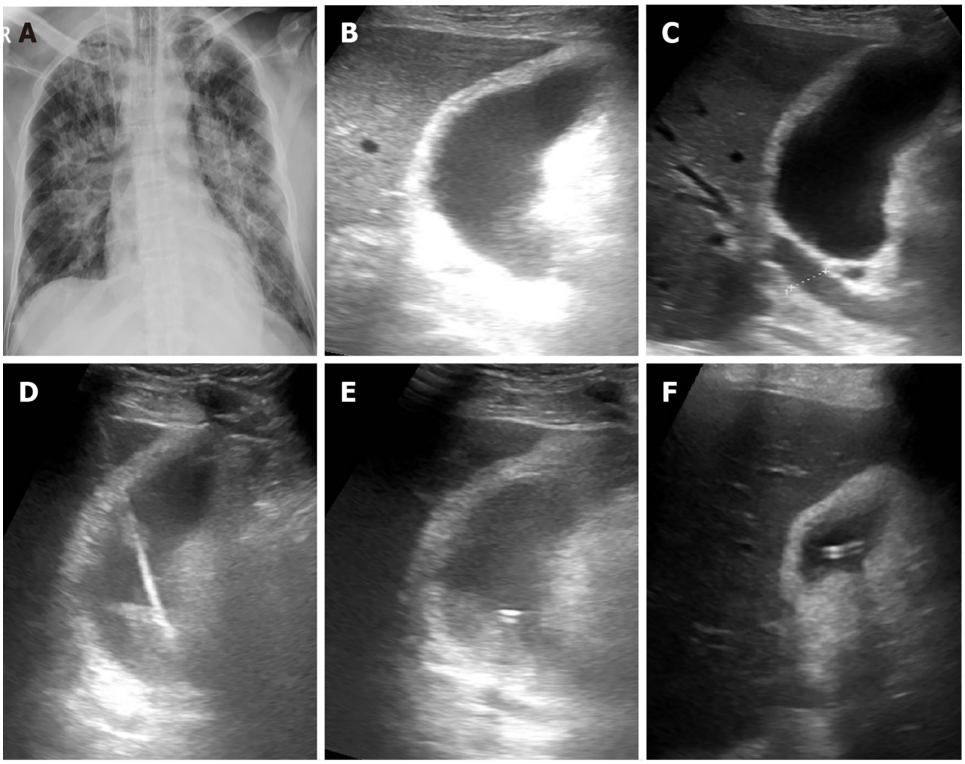

DOI: 10.4329/wjr.v14.i4.91

Figure 2 Cholecystostomy in a 72-yr-old male presented by acute cholecystitis. A: Frontal chest X-ray shows opacities involving both lungs with central predominance; B and C: B-mode ultrasound images show distended thick-walled gall bladder with biliary dilatation; D: B-mode ultrasound image show puncture needle through the gall bladder; E: B-mode ultrasound image tube inside the gall bladder; F: B-mode ultrasound image of the gall bladder after drainage.

percutaneous drainage procedures. The average volume of the drained fluid immediately after tube insertion was 85 mL. The average duration of drainage was 16 d. Follow-up scans showed a reduction of the retained content and associated inflammatory changes after tube insertion in all patients. Patient demographics, comorbidities, and outcomes are listed in Table 1.

The nature of drained fluid was reported in all cases. The fluid was reported as "dark green" or "pus" in cholecystostomy cases, "serosanguinous" and "infected bile" in complicated hepatic resection cases, "brownish" in the peripancreatic collection, "clotted blood" in the hepatic abscess, and "pus" in the

Table 1 Patients' demographics, comorbidities and outcome

	Cause of sepsis	Procedures	Age (yr)	Sex	Presentation	Co-morbidities	Ventilator	Tracheostomy	Outcome
Patient 1	Acute cholecystitis	Cholecystostomy	72	Male	Fever	IHD. AKI	40 d before drain	20 d before drain	Died 8 d post drain
Patient 2	Cholangitis and cholecystitis	Cholecystostomy	61	Male	Fever	Jaundice. AKI (on dialysis)	1 d before drain	12 d post drain	Died 16 d post drain
Patient 3	Acute cholecystitis	Cholecystostomy	55	Male	Abdominal pain	DM	No	No	Discharged 4 d post drain.
Patient 4	Post-operative biliary leakage resection of hemangioma	U/S guided drain	48	Female	Fever	DM. Septic shock	10 d post drain	No	Died 12 d post drain
Patient 5	Post-operative biliary leakage after liver resection for transplant	U/S guided drain	30	Male	Fever	No	No	No	Discharged 18 d post drain
Patient 6	Acute pancreatitis	CT-guided drain and EUS cystogast-rostomy	43	Male	Abdominal pain	HTN. Hyperlip-idemia	27 d post drain	No	Died 28 d post drain
Patient 7	Acute pancreatitis	U/S guided drain	41	Male	Abdominal pain	GB stones. Biliary obst. AKI	No	No	Discharged 10 d post drain
Patient 8	Recurrent hepatic abscess after surgical evacuation	U/S guided drain (2 tubes)	63	Male	Abdominal pain	DM. AKI	1 d before drain	1 d before drain	Died 19 d post drain
Patient 9	Right ilio-psoas and perivetebral abscesses	CT-guided drain then tube upsizing	60	Male	Abdominal pain	HTN. DM, AKI	3 d before drain	7 d post drain	Died 13 d post drain
Patient 10	Left lumbar region abscess and unhealthy sigmoid colon	CT-guided drainage. Sigmoid resection	31	Male	Abdominal pain and distension	Crohn's disease. Achalasia. GJ. Esophageal dilatation	No	No	Clinical failure after 18 d followed by another tube insertion and sigmoid resection. Discharged 48 d
Patient 11	Right pyelonephritis	Rt PCN	30	Male	Abdominal pain	Right hemicolectomy	No	No	Discharged 9 d post drain. Recurrence after 39 d and managed by tube exchange

U/S: Ultrasonography; EUS: Endoscopic ultrasound; PCN: Percutaneous nephrostomy; IHD: Ischemic heart disease; AKI: Acute kidney injury; DM: Diabetes mellitus; HTN: Hypertension; GB: Gall bladder; GJ: Gastrojejunostomy.

other collections. After all procedures, samples from drained fluid samples were sent for microbial analysis. Peripheral blood culture was performed for 9 out of 11 patients. In three cases (27.3%), fluid culture results were negative for bacterial growth; however, in one of them, the peripheral blood culture was positive for *Klebsiella* pneumonia. Eight cases (72.7%) were found to have positive fluid culture, with Escherichia coli being the most common isolated pathogen followed by *Klebsiella* pneumonia.

Only three patients had imaging features of severe pulmonary parenchymal disease attributed to COVID-19 at drainage tome, nevertheless three other patients were admitted to ICU and put under ventilator due to progression of respiratory symptoms. The parenchymal lesions were ground-glass opacities and consolidations with the basal and peripheral predominant distribution. In addition, pleural effusion was reported in three patients. The median time between confirmed diagnosis of COVID-19 by RT-PCR test and drainage of septic complications (time to drainage) was 8 d (range 0 d to 48 d). Table 2 shows data of drainage procedure, drained fluid, outcome, and chest imaging.

The mean WBCs and neutrophil counts show reduction 1 d and 7 d after drainage however there was no significant statistical difference (P = 0.6) between the mean of WBCs count before drainage (15.4 × 10^9/L) and seven days after drainage (12.1 × 10^9/L) and between the mean count of neutrophil (P = 0.4) before drainage (82.8 × 10^9/L) and seven days after drainage (70.9 × 10^9/L). The lymphocyte count

Table 2 Data of drainage procedure, drained fluid, and chest imaging

	IR procedure	Drain	Guide	Puncture	Drained fluid	Culture		Chest imaging	COVID-19 severity	Lesion distribution	Time between PCR test and drainage
						Drain	Peripheral blood				
Patient 1	Cholecystostomy	1 (8 Fr)	U/S	18G needle	Dark green	-ve	MDR (*Klebsiella*)	X-ray	Severe	Bilateral consolidation	48 d
Patient 2	Cholecystostomy	1 (8 Fr)	U/S	18G needle	Dark green	*E.coli* and *Klebsiella* pneumoniae	-ve	CT	Mild	Bilateral basal GGO with minimal effusion	3 d
Patient 3	Cholecystostomy	1 (8 Fr)	U/S	18G needle	Pus	*P. aeruginoa*. MRSA. *E.coli*	-ve	X-ray	Normal	Normal	5 d
Patient 4	Percutaneous drainage	1 (10 Fr)	U/S	18G needle	Infected bile	*E.coli*	-ve	CT	Sever	Bilateral consolidation with mild effusion	8 d
Patient 5	Percutaneous drainage	1 (8 Fr)	U/S	18G needle	Sero-sanginous	-ve	-ve	CT	Mild	Mild right pleural effusion	3 d
Patient 6	Percutaneous drainage	1 (10 Fr)	CT	21G needle	Brownish	*E.coli* and *Klebsiella* pneumoniae	-ve	CT	Mild	Left minimal effusion and basal GGO	17 d
Patient 7	Percutaneous drainage	1 (8 Fr)	CT	18G needle	Brownish	*E.coli*	-ve	CT	Mild	Bilateral basal GGO	2 d
Patient 8	Percutaneous drainage	2 (8 Fr)	U/S	18G needle	Clotted blood	-ve	-ve	X-ray	Normal	Mild right side pleural effusion	9 d
Patient 9	Percutaneous drainage	1 (10 Fr). 1 (8 Fr)	CT and US	21G needle	Pus	MRSA and staph aureus	-ve	CT	Severe	Bilateral GGO and consolidations	15 d
Patient 10	Percutaneous drainage	2 (8 Fr)	CT	21G needle	Pus	*E.coli* and *Ent. Foecalis*	NA	CT	Mild	Right side GGO	0 d
Patient 11	Right PCN	2 (8 Fr)	U/S and fluoro	21G needle	Pus	*Klebsiella* pneumoniae	-ve	X-ray	Normal	Normal	12 d

CT: Computed tomography; U/S: Ultrasonography; GGO: Ground-glass opacity; NA: Not available.

shows significant increased seven days after drainage (P = 0.03). Five patients had AKI manifested by elevation of the serum creatinine and urea levels. Total bilirubin level was elevated in eight patients and showed no significant reduction after drainage (P = 0.2). The CRP values were not significantly different (P = 0.06) before (182.0 mg/dL) and one week after tube insertion (133.0 mg/dL). Other inflammatory markers as D-dimer, procalcitonin and LDH were elevated in all patients before drainage and showed variable degree of non-statistically reduction and increase after drainage. The laboratory findings are listed in Table 3.

DISCUSSION

This study presents the clinical, radiological, and laboratory data for patients who underwent percutaneous drainage to manage septic complications associated with COVID-19 infection. The main finding is that patients with suspected septic complications associated with COVID-19 show relatively poor outcomes with 36.4% clinical success of percutaneous drainage despite 100% technical success. This finding was confirmed by the insignificant difference between the inflammatory markers before and after tube drainage insertion. Severe sepsis related to COVID-19 viral infection may be related to a decrease in mitochondrial efficiency and dysfunction of the respiratory chain[22,23]. In addition, autopsies have confirmed hyperinflammatory state with organ fibrosis, especially in high metabolic cells with high mitochondrial volume such as pneumocytes, endothelial cells, hepatocytes, and renal cells[24]. The resulting tissue hypoxia and increased inflammation, viral load, and other baseline risk factors contribute to an increased risk of severe sepsis or co-existed septic condition exaggeration.

Table 3 Median (inter-quartile range) for laboratory findings before drainage, 1 d and 7 d after drainage

	Pre drain	D1	D7	*P* value
WBCs × 10^9/L	15.4 (12.50-17.40)	18.8 (10.6-22.1)	12.1 (10.3-21.8)	0.656
Neutrophil × 10^9/L	82.8 (72.3-91.8)	86.6 (70.4-94.2)	70.9 (60.9-92.3)	0.091
Lymphocyte × 10^9/L	6.8 (3.7-9.9)	7.10 (2.8-11.2)	10.9 (2.9-19.2)	0.032[a]
CRP (mg/L)	182.0 (91.0-368.0)	166.0 (32.0-80.0)	133.0 (26.0-170.0)	0.061
Creatinine (μmol/L)	122.0 (70.0-353.0)	109.0 (54.0-426.0)	97.0 (56.0-364.0)	0.789
Urea (mmol/L)	9.2 (5.8-19.7)	8.6 (3.6-22.4)	9.1 (2.8-28.2)	0.574
Bilirubin (μmol/L)	19.1 (15.0-28.4)	14.4 (29.9-12.4)	15.5 (12.5-21.8)	0.247
D-Dimer (ng/mL)	1441.0 (620.0-3340.0)	1363.0 (460.0-2780.0)	1413.0 (380.0-3560.0)	0.373
Procalcitonin (ng/mL)	1.5 (1.1-3.0)	1.87 (0.85-3.56)	1.5800 (0.31-3.11)	0.398
LDH (IU/L)	359.0 (194.0-750.0)	397.0 (155.0-768.0)	438.0 (144.0-798.0)	0.929

[a]$P < 0.05$.

CRP: C-reactive protein; WBC: White blood cell; LDH: Lactate dehydrogenase.

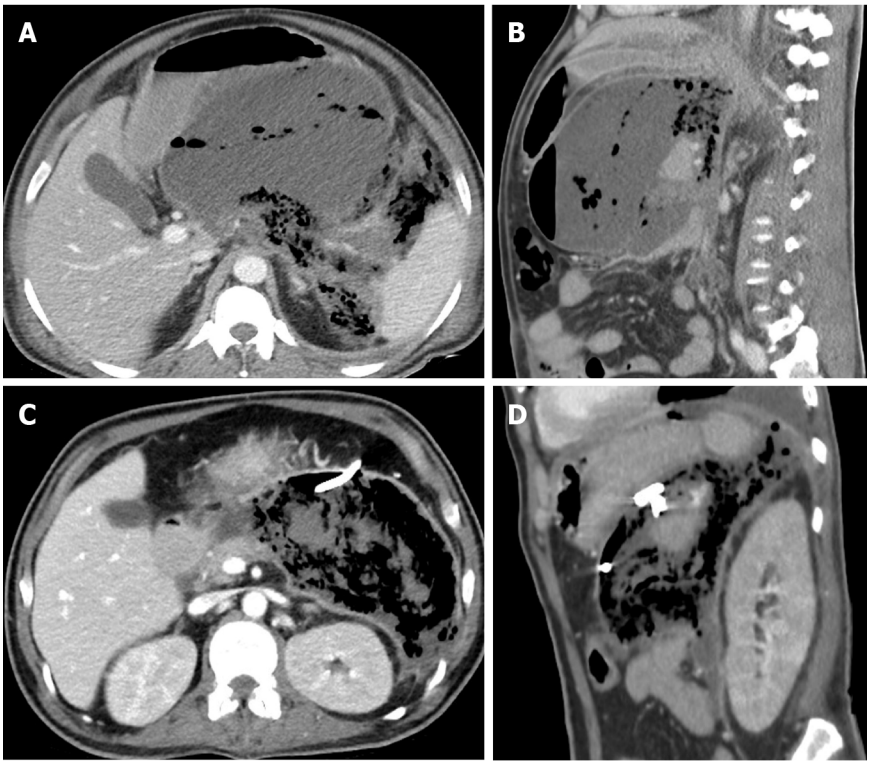

DOI: 10.4329/wjr.v14.i4.91

Figure 3 Percutaneous drainage of peripancreatic collection in a 43-yr-old male presented by acute pancreatitis. A and B: Axial and sagittal contrast enhanced computed tomography (CT) images show large peripancreatic collection/walled-off necrosis. The collection is mixed with pockets of gas inside and there is extension of the gas density into the retroperitoneal and perisplenic spaces; C and D: Axial and sagittal contrast enhanced CT images 22 d after tube insertion show reduction of the collection size with increased amount of gas within the collection.

This study included different types of septic complications as acute acalculous cholecystitis, acute pancreatitis, post-operative infection, abscesses in different locations, and acute pyelonephritis. Several reports described acute acalculous cholecystitis in COVID-19 patients[25-30] and raised the possibility of underlying dysregulated immune response or presence of viral RNA within the gall bladder wall as a culprit factor[28-30]. Percutaneous cholecystostomy for COVID-19 patients is recommended by multi-society position statement in case of surgical contraindication and after the failure of conservative therapy with antibiotics[31]. It is generally a preferred non-surgical procedure due to its relative safety, simplicity of execution, and reduced costs. Mattone *et al*[25] reported clinical failure of percutaneous

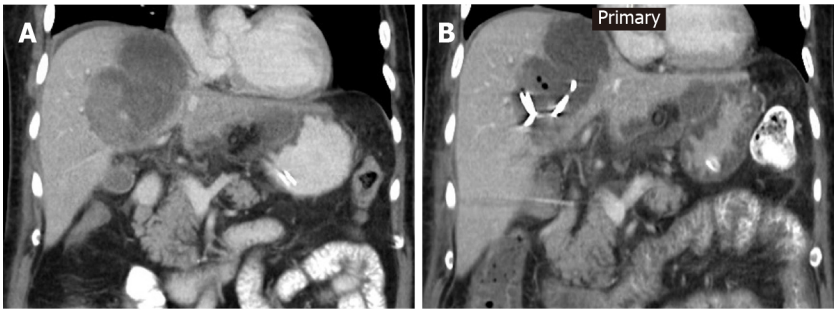

DOI: 10.4329/wjr.v14.i4.91

Figure 4 Percutaneous drainage of hepatic abscess in a 63-yr-old male. A: Coronal contrast enhanced computed tomography (CT) image shows thick-walled hepatic abscess with dependent high density inside secondary to clotted blood, a rim of perihepatic fluid is also noted; B: Coronal contrast enhanced CT image 6 d after tube insertion show reduction of the abscess size with few foci of gas density.

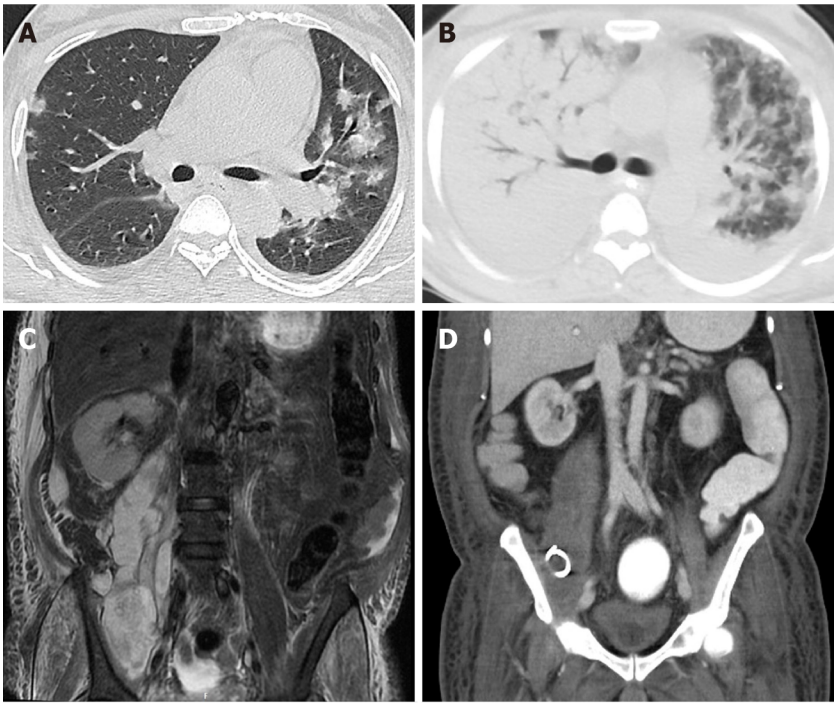

DOI: 10.4329/wjr.v14.i4.91

Figure 5 Percutaneous drainage of right psoas major abscess in a 60-yr-old male. A: Axial chest computed tomography (CT) image in pulmonary window shows bilateral ground-glass opacities (GGOs) and minimal bilateral pleural effusion; B: Axial chest CT image in pulmonary window 11 d after initial CT shows bilateral consolidation involving most of the right lung and GGOs in the remaining left lung parenchyma; C: Coronal T2 FAT SAT image shows large multi-locular psoas major abscess associated with muscular and subcutaneous soft tissue edema; D: Coronal contrast enhanced CT images 8 d after tube insertion show reduction of the collection size with regression of the associated soft tissue edema.

cholecystostomy after 3-d from tube insertion; the patient was shifted to surgery that revealed gangrenous cholecystitis. In this study, clinical success was reported only in one of three patients had cholecystostomy drainage of acute cholecystitis. Contrary to this result, cholecystostomy improved the clinical status of patients presented by acute acalculous cholecystitis co-existed with COVID-19[26,27]; however, the period of hospitalization was prolonged (25-67 d) compared to the mean hospitalization period in non-COVID-19 patients (10.5 d)[32].

COVID-19 associated pancreatic injury and acute pancreatitis are thought to be a result of direct cytopathic effect mediated by local viral replication or indirect mechanism related to either a systemic response to a harmful immune response or respiratory failure induced by the SARS-CoV-2[33]. COVID-19 patients with acute pancreatitis are more likely to experience admission to the ICU, peripancreatic fluid collections, pancreatic necrosis, persistent organ failure, prolonged hospital stay, and higher than usually reported 30-d mortality[34]. We encountered two cases of pancreatitis in the current study, one of them died 28 days after drainage.

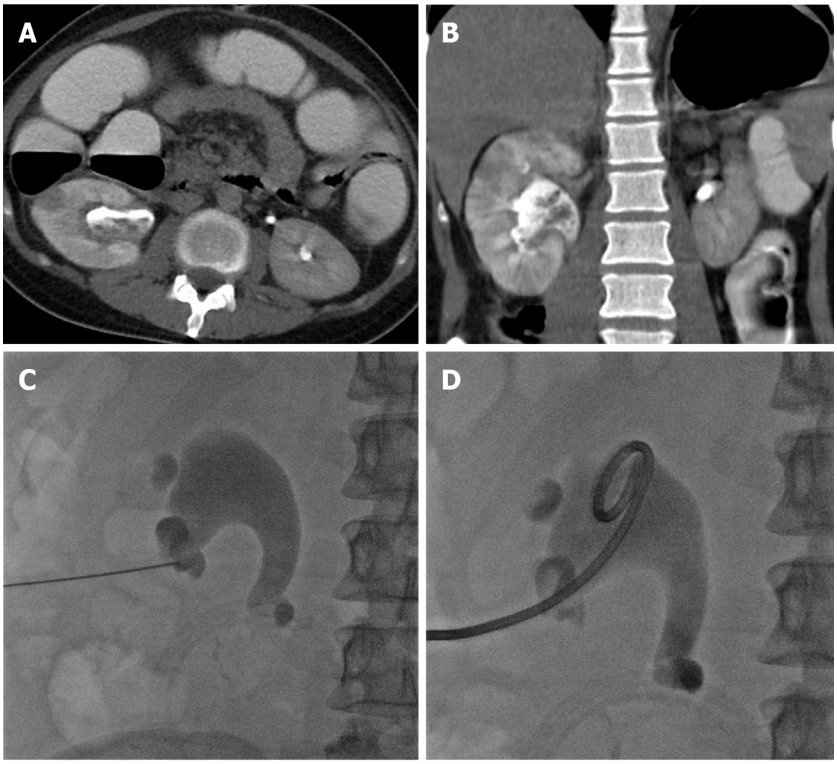

DOI: 10.4329/wjr.v14.i4.91

Figure 6 Percutaneous nephrostomy in a 30-yr-old male presented with acute pyelonephritis. A and B: Axial and coronal computed tomography images in excretory phase show characteristic features of acute pyelonephritis in the form of focal hypoenhnacing areas (striated nephrogram) and debris in dilated renal pelvis; C and D: Frontal fluoroscopic images show puncture needle in the lower calyces and successful insertion of nephrostomy tube.

In a meta-analysis performed by Abate *et al*[35], twenty-three articles with 2947 participants were included. The meta-analysis showed a very high global rate of postoperative mortality among COVID-19 patients of 20%. Percutaneous drainage was performed for two patients after complicated hepatic resection for hemangioma and liver donor, only the second patient survived and was discharged 18 days after drainage. The good outcome in this patient is attributed to the non-inflammatory nature of the drained fluid, lower inflammatory marker and less severity of COVID-19 as compared to the other patient.

Hepatic abscesses have been described in association with COVID-19[36,37]. While García Virosta *et al*[36] reported clinically successful percutaneous drainage for hepatic abscess and patient discharge after ten days from tube insertion, Elliot *et al*[37] reported a rapidly progressive severe acute respiratory distress syndrome, which was complicated by multiorgan failure and severe sepsis that ended by death after percutaneous drainage of hepatic abscess in a patient with COVID-19. One patient in this study presented with a large lumbar region abscess secondary to sigmoid colon perforation as proved by laparotomy. Bowel perforation secondary to COVID-19 has been attributed to microcirculation thrombosis[38] or direct insult to the colonic cells by the SARS-CoV-2 itself[39].

There is scanty literature on the association between COVID-19 and acute pyelonephritis. van 't Hof *et al*[40] described an unusual course of acute pyelonephritis in a young female with persistent fever and multiple blood clotting and hemorrhagic events one week after recovery from COVID-19. Similar to our results, pyelonephritis was managed successfully by percutaneous nephrostomy. More frequently, AKI is encountered among critically ill patients with COVID-19, affecting approximately 20%-40% of patients admitted to the hospital and particularly to the ICU[41]. AKI was the most frequent comorbidity (5/11) in this study. A significantly higher in-hospital death rate for patients with kidney abnormalities and AKI was reported by a study consisting of 701 SARS-CoV-2 positive patients[42].

COVID-19 requires a multidisciplinary approach to treatment with interventional radiology procedures that have contributed to worldwide patient care. In a study consisting of 92 patients who underwent 124 interventional procedures[43] [abscess drainage (12), percutaneous cholecystostomy (8), and nephrostomy tube (4)], the mortality rate in this study was 16.3 % (15/92). However, there was no specific data as regards clinical, laboratory, and radiological data of the included patients or correlation between specific IR procedures and mortality. In this study the poor outcome was related to the combined burden of severe COVID-19 pneumonia, presence of other co-morbidities and extent of sepsis.

This study has several limitations. First, our study cohort is small. Second, this study was retrospective in nature. Third, our results were not compared to a negative SARS-CoV-2 group with matched age, complication, and comorbidities; this may have overestimated the poor outcome of percutaneous drainage in this study group.

CONCLUSION

The current study demonstrates relatively poor clinical outcomes for patients having suspected septic complications associated with COVID-19 despite technically successful tube drainage and adequate antibiotic therapy. This study emphasizes the need for a large-scale comparative study on the relationship between septic complications, COVID-19, and comorbidities that might lead to poor clinical outcomes and clarifies the necessary precautions for percutaneous drainage in such patients.

ARTICLE HIGHLIGHTS

Research background

The resulting tissue hypoxia and increased inflammation secondary to severe coronavirus disease 2019 (COVID-19) combined with viral load, and other baseline risk factors contribute to an increased risk of severe sepsis or co-existed septic condition exaggeration.

Research motivation

We performed percutaneous drainage for septic complications of COVID-19 and wanted to report our experience.

Research objectives

To describe the clinical, radiological, and laboratory characteristics of a small cohort of patients infected by severe acute respiratory syndrome coronavirus 2 who underwent percutaneous drainage for septic complications and their post-procedural outcomes.

Research methods

This retrospective study consisted of 11 patients who were confirmed to have COVID-19 by RT-PCR test and required drain placement for septic complications. The mean age ± SD of the patients was 48.5 ± 14 years (range 30-72 years). Three patients underwent cholecystostomy for acute acalculous cholecystitis. Percutaneous drainage was performed in seven patients; two peripancreatic collections; two infected leaks after hepatic resection; one recurrent hepatic abscess, one psoas abscess and one lumbar abscess. One patient underwent a percutaneous nephrostomy for acute pyelonephritis.

Research results

Technical success was achieved in 100% of patients, while clinical success was achieved in 4 out of 11 patients (36.3%). Six patients (54.5%) died despite proper percutaneous drainage and adequate antibiotic coverage. One patient (9%) needed operative intervention. Two patients (18.2%) had two drainage procedures to drain multiple fluid collections. Two patients (18.2%) had repeat drainage procedures due to recurrent fluid collections. The average volume of the drained fluid immediately after tube insertion was 85 mL. Follow-up scans show a reduction of the retained content and associated inflammatory changes after tube insertion in all patients. There was no significant statistical difference (P = 0.6 and 0.4) between the mean of WBCs and neutrophils count before drainage and seven days after drainage. The lymphocyte count shows significant increased seven days after drainage (P = 0.03).

Research conclusions

In this study, patients having septic complications associated with COVID-19 showed relatively poor clinical outcomes despite technically successful percutaneous drainage.

Research perspectives

Prospective, larger multicentric study is needed to validate our results.

FOOTNOTES

Author contributions: Deif MA and Elmokadem AH designed the research study; Deif MA and Mounir AM performed the research; Elmokadem AH, Abo-Hedibah SA and Abdel Khalek AM analyzed the data and wrote the manuscript; all authors have read and approved the final manuscript.

Institutional review board statement: The study was reviewed and approved by the Mansoura university Institutional Review Board (R.21.12-1545).

Informed consent statement: A local institutional review board approved this retrospective study, and waivers of consent of medical record review were received.

Conflict-of-interest statement: All authors declare no conflict of interest.

Data sharing statement: Technical appendix, statistical code, and dataset available from the corresponding author at mokadem83@yahoo.com.

Country/Territory of origin: Egypt

ORCID number: Mohamed A Deif 0000-0002-8486-2622; Ahmad M Mounir 0000-0002-3322-7960; Sherif A Abo-Hedibah 0000-0002-1863-9828; Ahmed M Abdel Khalek 0000-0002-7751-7660; Ali H Elmokadem 0000-0001-5119-9548.

S-Editor: Gao CC
L-Editor: A
P-Editor: Gao CC

REFERENCES

1 **Singer M**, Deutschman CS, Seymour CW, Shankar-Hari M, Annane D, Bauer M, Bellomo R, Bernard GR, Chiche JD, Coopersmith CM, Hotchkiss RS, Levy MM, Marshall JC, Martin GS, Opal SM, Rubenfeld GD, van der Poll T, Vincent JL, Angus DC. The Third International Consensus Definitions for Sepsis and Septic Shock (Sepsis-3). *JAMA* 2016; **315**: 801-810 [PMID: 26903338 DOI: 10.1001/jama.2016.0287]

2 **Carter C**, Notter J. COVID-19 disease: a critical care perspective. *Clin Integr Care* 2020; **1**: 100003

3 **Quah P**, Li A, Phua J. Mortality rates of patients with COVID-19 in the intensive care unit: a systematic review of the emerging literature. *Crit Care* 2020; **24**: 285 [PMID: 32498689 DOI: 10.1186/s13054-020-03006-1]

4 **Mehta P**, McAuley DF, Brown M, Sanchez E, Tattersall RS, Manson JJ; HLH Across Speciality Collaboration, UK. COVID-19: consider cytokine storm syndromes and immunosuppression. *Lancet* 2020; **395**: 1033-1034 [PMID: 32192578 DOI: 10.1016/S0140-6736(20)30628-0]

5 **Ding R**, Meng Y, Ma X. The Central Role of the Inflammatory Response in Understanding the Heterogeneity of Sepsis-3. *Biomed Res Int* 2018; **2018**: 5086516 [PMID: 29977913 DOI: 10.1155/2018/5086516]

6 **Nedeva C**, Menassa J, Puthalakath H. Sepsis: Inflammation Is a Necessary Evil. *Front Cell Dev Biol* 2019; **7**: 108 [PMID: 31281814 DOI: 10.3389/fcell.2019.00108]

7 **Gentile LF**, Cuenca AG, Efron PA, Ang D, Bihorac A, McKinley BA, Moldawer LL, Moore FA. Persistent inflammation and immunosuppression: a common syndrome and new horizon for surgical intensive care. *J Trauma Acute Care Surg* 2012; **72**: 1491-1501 [PMID: 22695412 DOI: 10.1097/TA.0b013e318256e000]

8 **Rosenthal MD**, Kamel AY, Rosenthal CM, Brakenridge S, Croft CA, Moore FA. Chronic Critical Illness: Application of What We Know. *Nutr Clin Pract* 2018; **33**: 39-45 [PMID: 29323761 DOI: 10.1002/ncp.10024]

9 **Liu Y**, Mao B, Liang S, Yang JW, Lu HW, Chai YH, Wang L, Zhang L, Li QH, Zhao L, He Y, Gu XL, Ji XB, Li L, Jie ZJ, Li Q, Li XY, Lu HZ, Zhang WH, Song YL, Qu JM, Xu JF; Shanghai Clinical Treatment Experts Group for COVID-19. Association between age and clinical characteristics and outcomes of COVID-19. *Eur Respir J* 2020; **55** [PMID: 32312864 DOI: 10.1183/13993003.01112-2020]

10 **Thomas-Rüddel D**, Winning J, Dickmann P, Ouart D, Kortgen A, Janssens U, Bauer M. [Coronavirus disease 2019 (COVID-19): update for anesthesiologists and intensivists March 2020]. *Anaesthesist* 2020; **69**: 225-235 [PMID: 32189015 DOI: 10.1007/s00101-020-00758-x]

11 **Alhazzani W**, Møller MH, Arabi YM, Loeb M, Gong MN, Fan E, Oczkowski S, Levy MM, Derde L, Dzierba A, Du B, Aboodi M, Wunsch H, Cecconi M, Koh Y, Chertow DS, Maitland K, Alshamsi F, Belley-Cote E, Greco M, Laundy M, Morgan JS, Kesecioglu J, McGeer A, Mermel L, Mammen MJ, Alexander PE, Arrington A, Centofanti JE, Citerio G, Baw B, Memish ZA, Hammond N, Hayden FG, Evans L, Rhodes A. Surviving Sepsis Campaign: guidelines on the management of critically ill adults with Coronavirus Disease 2019 (COVID-19). *Intensive Care Med* 2020; **46**: 854-887 [PMID: 32222812 DOI: 10.1007/s00134-020-06022-5]

12 **Guan WJ**, Ni ZY, Hu Y, Liang WH, Ou CQ, He JX, Liu L, Shan H, Lei CL, Hui DSC, Du B, Li LJ, Zeng G, Yuen KY, Chen RC, Tang CL, Wang T, Chen PY, Xiang J, Li SY, Wang JL, Liang ZJ, Peng YX, Wei L, Liu Y, Hu YH, Peng P, Wang JM, Liu JY, Chen Z, Li G, Zheng ZJ, Qiu SQ, Luo J, Ye CJ, Zhu SY, Zhong NS; China Medical Treatment Expert Group for Covid-19. Clinical Characteristics of Coronavirus Disease 2019 in China. *N Engl J Med* 2020; **382**: 1708-1720 [PMID: 32109013 DOI: 10.1056/NEJMoa2002032]

13 **Huang C**, Wang Y, Li X, Ren L, Zhao J, Hu Y, Zhang L, Fan G, Xu J, Gu X, Cheng Z, Yu T, Xia J, Wei Y, Wu W, Xie X, Yin W, Li H, Liu M, Xiao Y, Gao H, Guo L, Xie J, Wang G, Jiang R, Gao Z, Jin Q, Wang J, Cao B. Clinical features of patients infected with 2019 novel coronavirus in Wuhan, China. *Lancet* 2020; **395**: 497-506 [PMID: 31986264 DOI: 10.1016/S0140-6736(20)30183-5]

14 **Wu Z**, McGoogan JM. Characteristics of and Important Lessons From the Coronavirus Disease 2019 (COVID-19) Outbreak in China: Summary of a Report of 72 314 Cases From the Chinese Center for Disease Control and Prevention. *JAMA* 2020; **323**: 1239-1242 [PMID: 32091533 DOI: 10.1001/jama.2020.2648]

15 **Elmokadem AH**, Batouty NM, Bayoumi D, Gadelhak BN, Abdel-Wahab RM, Zaky M, Abo-Hedibah SA, Ehab A, El-Morsy A. Mimickers of novel coronavirus disease 2019 (COVID-19) on chest CT: spectrum of CT and clinical features. *Insights Imaging* 2021; **12**: 12 [PMID: 33533965 DOI: 10.1186/s13244-020-00956-6]

16 **Elmokadem AH**, Bayoumi D, Abo-Hedibah SA, El-Morsy A. Diagnostic performance of chest CT in differentiating COVID-19 from other causes of ground-glass opacities. *EJRN* 2021; **52**: 1-10 [DOI: 10.1186/s43055-020-00398-6]

17 **Penn R**, David-Sanchez RY, Long J, Barclay W. Aberrant RNA replication products of highly pathogenic avian influenza viruses and its impact in the mammalian associated cytokine storm. *Access Microbiol* 2019; **1** [DOI: 10.1099/acmi.ac2019.po0457]

18 **Spencer JV**, Religa P, Lehmann MH. Editorial: Cytokine-Mediated Organ Dysfunction and Tissue Damage Induced by Viruses. *Front Immunol* 2020; **11**: 2 [PMID: 32038654 DOI: 10.3389/fimmu.2020.00002]

19 **Boomer JS**, To K, Chang KC, Takasu O, Osborne DF, Walton AH, Bricker TL, Jarman SD 2nd, Kreisel D, Krupnick AS, Srivastava A, Swanson PE, Green JM, Hotchkiss RS. Immunosuppression in patients who die of sepsis and multiple organ failure. *JAMA* 2011; **306**: 2594-2605 [PMID: 22187279 DOI: 10.1001/jama.2011.1829]

20 **Zhou F**, Yu T, Du R, Fan G, Liu Y, Liu Z, Xiang J, Wang Y, Song B, Gu X, Guan L, Wei Y, Li H, Wu X, Xu J, Tu S, Zhang Y, Chen H, Cao B. Clinical course and risk factors for mortality of adult inpatients with COVID-19 in Wuhan, China: a retrospective cohort study. *Lancet* 2020; **395**: 1054-1062 [PMID: 32171076 DOI: 10.1016/S0140-6736(20)30566-3]

21 **Abo-Hedibah SA**, Tharwat N, Elmokadem AH. Is chest X-ray severity scoring for COVID-19 pneumonia reliable? *Pol J Radiol* 2021; **86**: e432-e439 [PMID: 34429790 DOI: 10.5114/pjr.2021.108172]

22 **Brealey D**, Brand M, Hargreaves I, Heales S, Land J, Smolenski R, Davies NA, Cooper CE, Singer M. Association between mitochondrial dysfunction and severity and outcome of septic shock. *Lancet* 2002; **360**: 219-223 [PMID: 12133657 DOI: 10.1016/S0140-6736(02)09459-X]

23 **Singer M**. The role of mitochondrial dysfunction in sepsis-induced multi-organ failure. *Virulence* 2014; **5**: 66-72 [PMID: 24185508 DOI: 10.4161/viru.26907]

24 **Shenoy S**. Coronavirus (Covid-19) sepsis: revisiting mitochondrial dysfunction in pathogenesis, aging, inflammation, and mortality. *Inflamm Res* 2020; **69**: 1077-1085 [PMID: 32767095 DOI: 10.1007/s00011-020-01389-z]

25 **Mattone E**, Sofia M, Schembari E, Palumbo V, Bonaccorso R, Randazzo V, La Greca G, Iacobello C, Russello D, Latteri S. Acute acalculous cholecystitis on a COVID-19 patient: a case report. *Ann Med Surg (Lond)* 2020; **58**: 73-75 [PMID: 32895611 DOI: 10.1016/j.amsu.2020.08.027]

26 **Ying M**, Lu B, Pan J, Lu G, Zhou S, Wang D, Li L, Shen J, Shu J; From the COVID-19 Investigating and Research Team. COVID-19 with acute cholecystitis: a case report. *BMC Infect Dis* 2020; **20**: 437 [PMID: 32571224 DOI: 10.1186/s12879-020-05164-7]

27 **Wahid N**, Bhardwaj T, Borinsky C, Tavakkoli M, Wan D, Wong T. Acute Acalculous Cholecystitis During Severe COVID-19 Hospitalizations. *Am J Gastroenterol* 2020; **115**: S794 [DOI: 10.14309/01.ajg.0000708300.51603.f0]

28 **Alhassan SM**, Iqbal P, Fikrey L, Mohamed Ibrahim MI, Qamar MS, Chaponda M, Munir W. Post COVID 19 acute acalculous cholecystitis raising the possibility of underlying dysregulated immune response, a case report. *Ann Med Surg (Lond)* 2020; **60**: 434-437 [PMID: 33224493 DOI: 10.1016/j.amsu.2020.11.031]

29 **Bruni A**, Garofalo E, Zuccalà V, Currò G, Torti C, Navarra G, De Sarro G, Navalesi P, Longhini F, Ammendola M. Histopathological findings in a COVID-19 patient affected by ischemic gangrenous cholecystitis. *World J Emerg Surg* 2020; **15**: 43 [PMID: 32615987 DOI: 10.1186/s13017-020-00320-5]

30 **Balaphas A**, Gkoufa K, Meyer J, Peloso A, Bornand A, McKee TA, Toso C, Popeskou SG. COVID-19 can mimic acute cholecystitis and is associated with the presence of viral RNA in the gallbladder wall. *J Hepatol* 2020; **73**: 1566-1568 [PMID: 32890595 DOI: 10.1016/j.jhep.2020.08.020]

31 **Campanile FC**, Podda M, Arezzo A, Botteri E, Sartori A, Guerrieri M, Cassinotti E, Muttillo I, Pisano M, Brachet Contul R, D'Ambrosio G, Cuccurullo D, Bergamini C, Allaix ME, Caracino V, Petz WL, Milone M, Silecchia G, Anania G, Agrusa A, Di Saverio S, Casarano S, Cicala C, Narilli P, Federici S, Carlini M, Paganini A, Bianchi PP, Salaj A, Mazzari A, Meniconi RL, Puzziello A, Terrosu G, De Simone B, Coccolini F, Catena F, Agresta F. Acute cholecystitis during COVID-19 pandemic: a multisocietary position statement. *World J Emerg Surg* 2020; **15**: 38 [PMID: 32513287 DOI: 10.1186/s13017-020-00317-0]

32 **Popowicz A**, Lundell L, Gerber P, Gustafsson U, Pieniowski E, Sinabulya H, Sjödahl K, Tsekrekos A, Sandblom G. Cholecystostomy as Bridge to Surgery and as Definitive Treatment or Acute Cholecystectomy in Patients with Acute Cholecystitis. *Gastroenterol Res Pract* 2016; **2016**: 3672416 [PMID: 26839538 DOI: 10.1155/2016/3672416]

33 **Wang F**, Wang H, Fan J, Zhang Y, Zhao Q. Pancreatic Injury Patterns in Patients With Coronavirus Disease 19 Pneumonia. *Gastroenterology* 2020; **159**: 367-370 [PMID: 32247022 DOI: 10.1053/j.gastro.2020.03.055]

34 **Pandanaboyana S**, Moir J, Leeds JS, Oppong K, Kanwar A, Marzouk A, Belgaumkar A, Gupta A, Siriwardena AK, Haque AR, Awan A, Balakrishnan A, Rawashdeh A, Ivanov B, Parmar C, M Halloran C, Caruana C, Borg CM, Gomez D, Damaskos D, Karavias D, Finch G, Ebied H, K Pine J, R A Skipworth J, Milburn J, Latif J, Ratnam Apollos J, El Kafsi J, Windsor JA, Roberts K, Wang K, Ravi K, V Coats M, Hollyman M, Phillips M, Okocha M, Sj Wilson M, A Ameer N, Kumar N, Shah N, Lapolla P, Magee C, Al-Sarireh B, Lunevicius R, Benhmida R, Singhal R, Balachandra S, Demirli Atıcı S, Jaunoo S, Dwerryhouse S, Boyce T, Charalampakis V, Kanakala V, Abbas Z, Nayar M; COVID PAN collaborative group. SARS-CoV-2 infection in acute pancreatitis increases disease severity and 30-day mortality: COVID PAN collaborative study. *Gut* 2021; **70**: 1061-1069 [PMID: 33547182 DOI: 10.1136/gutjnl-2020-323364]

35 **Abate SM**, Mantefardo B, Basu B. Postoperative mortality among surgical patients with COVID-19: a systematic review and meta-analysis. *Patient Saf Surg* 2020; **14**: 37 [PMID: 33062056 DOI: 10.1186/s13037-020-00262-6]

36 **García Virosta M**, Ortega I, Ferrero E, Picardo AL. Diagnostic Delay During the COVID-19 Pandemic: Liver Abscess Secondary to Acute Lithiasic Cholecystitis. *Cir Esp (Engl Ed)* 2020; **98**: 409 [PMID: 32408994 DOI: 10.1016/j.ciresp.2020.04.010]

37 **Elliott R**, Ohene Baah N, Grossman VA, Sharma AK. COVID-19 Related Mortality During Management of a Hepatic Abscess. *J Radiol Nurs* 2020; **39**: 271-274 [PMID: 32982611 DOI: 10.1016/j.jradnu.2020.09.001]

38 **Nahas SC**, Meira-JÚnior JD, Sobrado LF, Sorbello M, Segatelli V, Abdala E, Ribeiro-JÚnior U, Cecconello I. Intestinal perforation caused by COVID-19. *Arq Bras Cir Dig* 2020; **33**: e1515 [PMID: 33237160 DOI: 10.1590/0102-672020190001e1515]

39 **De Nardi P**, Parolini DC, Ripa M, Racca S, Rosati R. Bowel perforation in a Covid-19 patient: case report. *Int J Colorectal Dis* 2020; **35**: 1797-1800 [PMID: 32458395 DOI: 10.1007/s00384-020-03627-6]

40 **van 't Hof LJ**, Pellikaan L, Soonawala D, Roshani H. An Unusual Presentation of Pyelonephritis: Is It COVID-19 Related? *SN Compr Clin Med* 2021; 1-6 [PMID: 33937632 DOI: 10.1007/s42399-021-00909-0]

41 **Revzin MV**, Raza S, Srivastava NC, Warshawsky R, D'Agostino C, Malhotra A, Bader AS, Patel RD, Chen K, Kyriakakos C, Pellerito JS. Multisystem Imaging Manifestations of COVID-19, Part 2: From Cardiac Complications to Pediatric Manifestations. *Radiographics* 2020; **40**: 1866-1892 [PMID: 33136488 DOI: 10.1148/rg.2020200195]

42 **Cheng Y**, Luo R, Wang K, Zhang M, Wang Z, Dong L, Li J, Yao Y, Ge S, Xu G. Kidney disease is associated with in-hospital death of patients with COVID-19. *Kidney Int* 2020; **97**: 829-838 [PMID: 32247631 DOI: 10.1016/j.kint.2020.03.005]

43 **Lee KS**, Talenfeld AD, Browne WF, Holzwanger DJ, Harnain C, Kesselman A, Pua BB. Role of interventional radiology in the treatment of COVID-19 patients: Early experience from an epicenter. *Clin Imaging* 2021; **71**: 143-146 [PMID: 33259979 DOI: 10.1016/j.clinimag.2020.10.048]

World Journal of Radiology

Submit a Manuscript: https://www.f6publishing.com

World J Radiol 2022 April 28; 14(4): 104-106

DOI: 10.4329/wjr.v14.i4.104

ISSN 1949-8470 (online)

LETTER TO THE EDITOR

Follow-up computed tomography scan in post-COVID-19 pneumonia

Asad Chohan, Saiara Choudhury, Rahul Dadhwal, Abhay P Vakil, Rene Franco, Pahnwat Tonya Taweesedt

Specialty type: Radiology, nuclear medicine and medical imaging

Provenance and peer review: Unsolicited article; Externally peer reviewed.

Peer-review model: Single blind

Peer-review report's scientific quality classification

Grade A (Excellent): A
Grade B (Very good): B
Grade C (Good): C
Grade D (Fair): 0
Grade E (Poor): 0

P-Reviewer: Arteaga-Livias K, Peru; Naswhan AJ, Qatar; Valencia GA, Peru

Received: December 17, 2021
Peer-review started: December 17, 2021
First decision: February 21, 2022
Revised: February 24, 2022
Accepted: March 26, 2022
Article in press: March 26, 2022
Published online: April 28, 2022

Asad Chohan, Saiara Choudhury, Rahul Dadhwal, Abhay P Vakil, Rene Franco, Pahnwat Tonya Taweesedt, Pulmonary Medicine, Corpus Christi Medical Center, Corpus Christi, TX 78411, United States

Corresponding author: Pahnwat Tonya Taweesedt, MD, Academic Fellow, Pulmonary Medicine, Corpus Christi Medical Center, 3315 S Alameda St, Corpus Christi, TX 78411, United States. pahnwatt@gmail.com

Abstract

The coronavirus disease 2019 (COVID-19) global pandemic can be a severe illness that leads to morbidity and mortality. With the increasing number of COVID-19 pneumonia survivors, several long-term changes may persist, including abnormal imaging of lung parenchyma. In addition to the clinical course, it is vital to follow up on pulmonary imaging during the post-infectious period, which is not routinely required in other common pulmonary diagnoses. Computed tomography (CT) scan of the chest is an effective and diagnostic tool for pneumonia which gives an insight into structural abnormalities within the lungs, complications, and possible progression of the disease. Several studies have monitored COVID-19 pneumonia and its complications using serial CT chest imaging from the initial phase of infection, hospitalization, and post-discharge. Nonetheless, long-term follow-up imaging data in post-COVID-19 is still limited. We have summarized the findings utilizing a systematic review of the literature regarding COVID-19 pneumonia imaging, including long-term follow-up.

Key Words: COVID-19; Pneumonia; Computed tomography; Evolution; Progression

Core Tip: Changes seen in computed tomography imaging related to coronavirus disease 2019 (COVID-19) pneumonia appear to progress and peak around two weeks post-hospitalization. Overall improvement and complete resolution of COVID-19 pneumonia-related changes imaging can be seen in the majority of the patients with long-term follow-up. We have summarized the findings utilizing a systematic review of the literature regarding COVID-19 pneumonia imaging, including long-term follow-up.

Citation: Chohan A, Choudhury S, Dadhwal R, Vakil AP, Franco R, Taweesedt PT. Follow-up computed tomography scan in post-COVID-19 pneumonia. *World J Radiol* 2022; 14(4): 104-106
URL: https://www.wjgnet.com/1949-8470/full/v14/i4/104.htm
DOI: https://dx.doi.org/10.4329/wjr.v14.i4.104

TO THE EDITOR

We read the article titled "Review on radiological evolution of COVID-19 pneumonia using computed tomography" by Casartelli *et al*[1] with keen interest. A chest computed tomography (CT) scan can be a useful diagnostic tool in a high-prevalence or pandemic situation, especially with clinical correlation. Risk stratification and assessing the progression of disease are also effective uses of CT chest imaging in coronavirus disease 2019 (COVID-19) patients. Given the global spread of COVID-19 and the magnitude of both direct and indirect effects of the disease, a CT scan of the chest can help in long-term prognostication in patients who survive.

Multiple studies have concluded that with disease progression, certain initial CT findings in COVID-19 can evolve with a specific pattern and regularity. COVID-19 pneumonia-related changes seen on CT chest imaging typically progress rapidly, plateau, and subsequently start to resolve thereafter. Changes in CT imaging vary widely from six to seventeen days but typically stabilize within the first two weeks of COVID-19 pneumonia. In the short term, some of the features seem to recur, with scans mostly showing consolidations and ground-glass opacities (GGO). Besides GGO, chest CT characteristics that indicate the reparation, including subpleural, linear opacities, and fibrotic changes, were also reported. A sign termed "fishing net on trees" has also been reported. Some reports have also mentioned interseptal thickening and fibrous streaks[1,2]. Three weeks post-discharge, GGO and fibrous stripes have been seen, while after four weeks, mostly linear opacities remained. The "tinted" sign and bronchovascular bundle distortion have also been mentioned. The bronchovascular bundle distortion could possibly be a result of inflammatory destruction or subsegmental atelectasis. The latter two signs mentioned above may signify the gradual resolution of inflammation with re-expansion of alveoli based on previous reports. This review included reports with follow-up durations of up to four months[1].

In a study conducted by Pan *et al*[3], two hundred nine patients with COVID-19 infection, who had been admitted to the hospital, undertook serial chest CT at three, seven, and twelve months. One-year CT chest follow-up revealed residual linear lesions, multiple areas of reticular opacities/cysts, and complete resolution in 12%, 13%, and 75%, respectively[3]. In another study conducted by Guan *et al*[4], CT results of 69 patients who had COVID-19 infection were assessed in three different phases: Initial CT, peak CT, and CT prior to discharge. Peak CT in this study was the highest attenuation of the density without alteration in size during COVID-19 progression or the maximal size of lesion on CT which is the most common pattern. The intervals were closely correlated to lobe scores and CT appearances; the higher the lobe score, the longer the intervals. The lobe score was calculated according to the percentage of the lesion in one lobe with the zero equals to no lesion, one equals more than 0% to less than 25%, two equals 25% to less than 50%, three equals 50% to less than 75%, and four equals to 75% or more. While the utilization of lobe score may be beneficial, further studies are necessary to assess its effectiveness on a larger scale.

The duration of initial interval is inversely correlated with the amount of consolidations, air bronchograms, and irregular lines[3]. The intervals will be longer if irregular and reticular lines are seen on the peak CT and pre-discharge CT. After that, COVID-19 pneumonia lesions on the CT chest may resolve completely, while GGO, irregular and reticular lines may remain[3]. In a similar study conducted by Chen *et al*[5], 41 patients were followed with chest CT during the hospital stay and at two weeks, one month, three months, six months, and one year after discharge. The study concluded that patients showed continuous improvement on lung CT scans during the 1-year follow-up time; however residual lesions (GGO and reticular patterns) may still be found, which are associated with lung volume parameters and risk of developing lung opacities[5]. Liu *et al*[6] retrospectively evaluated chest CT follow-ups on 51 patients with COVID-19 performed on the day prior to discharge, two weeks post-discharge, and four weeks post-discharge. The results of this study indicated that changes seen were significantly reduced, including density reduction on follow-up scans as compared to the scans done at the time of discharge.

Unlike the systematic review by Casartelli *et al*[1], these results showed that 64.7% of discharged patients progressed to complete resolution of previously seen lung lesions at 4-wk follow-up, indicating that damaged lung tissue could heal in patients with COVID-19 pneumonia[5]. In another study conducted by Liu *et al*[7], 41 patients diagnosed with COVID-19 were followed up after seven months with chest CT and cardiopulmonary exercise testing. The predominant chest CT patterns at seven months included parenchymal bands (41%), interlobular septal thickening (32%), and traction bronchiectasis (29%). Sixty-one percent of the patients achieved complete radiological resolution, while 29% went on to develop pulmonary fibrosis. Those patients who went on to develop fibrotic lung disease appeared to have an increased risk due to older age and comorbid conditions[7].

While CT scan of the chest is an effective tool in COVID-19 patients, the side effects to patients of repeat irradiation need to be kept in mind and the use of low dose CT to follow up these patients can be considered. In conclusion, CT scans of the chest are an effective diagnostic tool which can provide insight into the structural pathology of pulmonary disease, its progression, and its association with long-term effects. Future studies should be utilized to define its utility in determining long-term progression in patients with COVID-19 pneumonia.

FOOTNOTES

Author contributions: Chohan A and Taweesedt PT wrote the letter; Choudhury S wrote the letter; Franco R, Dadhwal R, Vakil AP and Taweesedt PT revised the letter.

Conflict-of-interest statement: All authors declare no conflicts-of-interest related to this article.

Country/Territory of origin: United States

ORCID number: Asad Chohan 0000-0002-1801-9792; Saiara Choudhury 0000-0001-7225-4905; Rahul Dadhwal 0000-0001-6963-1466; Abhay P Vakil 0000-0003-4947-0233; Rene Franco 0000-0002-0684-7734; Pahnwat Tonya Taweesedt 0000-0002-5791-6920.

S-Editor: Wang JJ
L-Editor: A
P-Editor: Wang JJ

REFERENCES

1 **Casartelli C**, Perrone F, Balbi M, Alfieri V, Milanese G, Buti S, Silva M, Sverzellati N, Bersanelli M. Review on radiological evolution of COVID-19 pneumonia using computed tomography. *World J Radiol* 2021; **13**: 294-306 [PMID: 34630915 DOI: 10.4329/wjr.v13.i9.294]

2 **Mejía-Zambrano H**. Radiological and functional pulmonary complications in patients recovered from COVID-19. *Microb Infect Chemother* 2021 [DOI: 10.54034/mic.e1217]

3 **Pan F**, Yang L, Liang B, Ye T, Li L, Liu D, Wang J, Hesketh RL, Zheng C. Chest CT Patterns from Diagnosis to 1 Year of Follow-up in Patients with COVID-19. *Radiology* 2022; **302**: 709-719 [PMID: 34609153 DOI: 10.1148/radiol.2021211199]

4 **Guan CS**, Lv ZB, Li JJ, Du YN, Chen H, Cui T, Guo N, Chen BD, Xie RM. CT appearances, patterns of progression, and follow-up of COVID-19: evaluation on thin-section CT. *Insights Imaging* 2021; **12**: 73 [PMID: 34110540 DOI: 10.1186/s13244-021-01019-0]

5 **Chen Y**, Ding C, Yu L, Guo W, Feng X, Su J, Xu T, Ren C, Shi D, Wu W, Yi P, Liu J, Tao J, Lang G, Li Y, Xu M, Sheng J, Li L, Xu K. One-year follow-up of chest CT findings in patients after SARS-CoV-2 infection. *BMC Med* 2021; **19**: 191 [PMID: 34365975 DOI: 10.1186/s12916-021-02056-8]

6 **Liu C**, Ye L, Xia R, Zheng X, Yuan C, Wang Z, Lin R, Shi D, Gao Y, Yao J, Sun Q, Wang X, Jin M. Chest Computed Tomography and Clinical Follow-Up of Discharged Patients with COVID-19 in Wenzhou City, Zhejiang, China. *Ann Am Thorac Soc* 2020; **17**: 1231-1237 [PMID: 32692945 DOI: 10.1513/AnnalsATS.202004-324OC]

7 **Liu M**, Lv F, Huang Y, Xiao K. Follow-Up Study of the Chest CT Characteristics of COVID-19 Survivors Seven Months After Recovery. *Front Med (Lausanne)* 2021; **8**: 636298 [PMID: 33732719 DOI: 10.3389/fmed.2021.636298]

Published by **Baishideng Publishing Group Inc**
7041 Koll Center Parkway, Suite 160, Pleasanton, CA 94566, USA
Telephone: +1-925-3991568
E-mail: bpgoffice@wjgnet.com
Help Desk: https://www.f6publishing.com/helpdesk
https://www.wjgnet.com